The error kinematics in these two cases look quite different. Equations (3.47) or (3.48) involves the attitude error, while Eq. (3.50) involves the attitude estimate. The difference arises because either attitude dynamics or strapdown gyro measurements give the components of the body rate in the spacecraft body frame. If the attitude errors are specified in the body frame, there are two slightly different body frames, the true frame and the estimated frame. If the attitude errors are specified in the reference frame, on the other hand, there is only one body frame. The difference between the two formulations is purely kinematic, it has nothing to do with either frame being inertial or non-inertial.[1]

3.3 Attitude Dynamics

We now turn to attitude dynamics, emphasizing the fundamental role of angular momentum. We begin by defining the center of mass of a collection of mass points and showing how the rotational motion of this system can be treated separately from the motion of the center of mass. We then specialize to the case of a rigid body, defining the moment of inertia tensor and expressing the angular momentum and rotational kinetic energy in terms of the moment of inertia and the angular velocity. We collect the rotational equations of motion, kinematic and dynamic, in one place for easy reference, and then discuss the torque-free motion of a rigid body. Then we show how to include internal and external torques in the dynamics.

3.3.1 Angular Momentum and Kinetic Energy

We will consider a spacecraft (or anything else) to be made up of a collection of n point masses. The angular momentum with respect to the origin 0 of an inertial coordinate frame is defined in terms of the masses m_i, positions $\mathbf{r}^{i0}$, and velocities $\mathbf{v}^{i0} = \dot{\mathbf{r}}^{i0}$ of the points relative to 0 by

$$\mathbf{H}^0 \equiv \sum_{i=1}^{n} \mathbf{r}^{i0} \times m_i \mathbf{v}^{i0} \tag{3.51}$$

Newton's second law of motion tells us that $m_i \dot{\mathbf{v}}_I^{i0} = \mathbf{F}_I^i$ in an inertial reference frame, and $\mathbf{v}^{i0} \times \mathbf{v}^{i0} = 0$, so the angular momentum obeys the equation

$$\dot{\mathbf{H}}_I^0 = \sum_{i=1}^{n} \mathbf{r}_I^{i0} \times \mathbf{F}_I^i = \sum_{i=1}^{n} \mathbf{r}_I^{i0} \times \left(\sum_{j=1}^{n} \mathbf{F}_I^{ij} + \mathbf{F}_I^{iext} \right) \tag{3.52}$$

[1]The situation would be different if the gyros were used to stabilize a platform to serve as an inertially fixed reference, but such platforms are now used only infrequently in space.

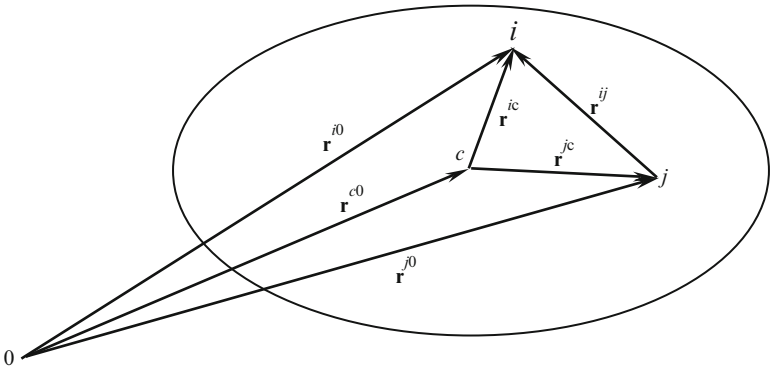

Fig. 3.1 Center of mass, c, and two representative mass points

where $\mathbf{F}^{ij}$ is the force exerted on mass point i by mass point j and $\mathbf{F}^{iext}$ is the force exerted on i by everything external to the system of mass points.[2] Any pair of mass points with indices k and ℓ appears twice in the double sum over i and j, as $\mathbf{r}_I^{k0} \times \mathbf{F}_I^{k\ell}$ and as $\mathbf{r}_I^{\ell 0} \times \mathbf{F}_I^{\ell k}$. Newton's third law of motion says that $\mathbf{F}^{\ell k} = -\mathbf{F}^{k\ell}$, so these two terms sum to $(\mathbf{r}_I^{k0} - \mathbf{r}_I^{\ell 0}) \times \mathbf{F}_I^{k\ell} = \mathbf{r}_I^{k\ell} \times \mathbf{F}_I^{k\ell}$. This geometry is illustrated in Fig. 3.1. We assume that the force between two mass points acts along the line between them, an assumption known as the *strong law of action and reaction* [10], so the cross product vanishes and

$$\dot{\mathbf{H}}_I^0 = \sum_{i=1}^{n} \mathbf{r}_I^{i0} \times \mathbf{F}_I^{iext} \equiv \mathbf{L}_I^0 \tag{3.53}$$

where $\mathbf{L}_I^0$ is the net torque about 0 exerted on the collection of mass points by all the external forces.[3] Note that internal forces give no contribution to the net torque.

We will now define the center of mass of the collection of mass points and prove the important result that the motion of the center of mass and the motion of the mass points about their center of mass are uncoupled. The location of the center of mass c with respect to the origin 0 is defined as

$$\mathbf{r}^{c0} \equiv \left(\sum_{i=1}^{n} m_i \mathbf{r}^{i0} \right) \Big/ M \tag{3.54}$$

where $M \equiv \sum_{i=1}^{n} m_i$ is the total mass of the collection of mass points. It follows from this definition that

$$\sum_{i=1}^{n} m_i \mathbf{r}^{ic} = \sum_{i=1}^{n} m_i (\mathbf{r}^{i0} - \mathbf{r}^{c0}) = M\mathbf{r}^{c0} - M\mathbf{r}^{c0} = \mathbf{0} \tag{3.55}$$

[2] We assume that $\mathbf{F}^{ii}$, the force exerted by a mass point on itself, is zero.

[3] Warning! Many authors use the letter $\mathbf{L}$ to denote angular momentum.

where these vectors are illustrated in Fig. 3.1. Using this result and its derivative, the angular momentum about the arbitrary point 0 can be written as the sum of the angular momentum about the center of mass and the angular momentum of the center-of-mass motion, namely

$$\begin{aligned}\mathbf{H}^0 &= \sum_{i=1}^{n} m_i(\mathbf{r}^{ic} + \mathbf{r}^{c0}) \times (\mathbf{v}^{ic} + \mathbf{v}^{c0}) = \sum_{i=1}^{n} m_i \mathbf{r}^{ic} \times \mathbf{v}^{ic} + \mathbf{r}^{c0} \times M\mathbf{v}^{c0} \\ &= \mathbf{H}^c + \mathbf{r}^{c0} \times M\mathbf{v}^{c0} \end{aligned} \tag{3.56}$$

The net torque can similarly be expressed as

$$\begin{aligned}\mathbf{L}^0 &= \sum_{i=1}^{n} (\mathbf{r}^{ic} + \mathbf{r}^{c0}) \times \mathbf{F}^{iext} = \sum_{i=1}^{n} \mathbf{r}^{ic} \times \mathbf{F}^{iext} + \mathbf{r}^{c0} \times \sum_{i=1}^{n} \mathbf{F}^{iext} \\ &= \mathbf{L}^c + \mathbf{r}^{c0} \times \mathbf{F} \end{aligned} \tag{3.57}$$

where $\mathbf{F}$ is the net external force on the collection of point masses. Now in an inertial frame, we have $\mathbf{F}_I = M\dot{\mathbf{v}}_I^{c0}$, so substituting Eqs. (3.56) and (3.57) into Eq. (3.53) and canceling the term due to motion of the center of mass gives *Euler's equation*

$$\dot{\mathbf{H}}_I^c = \mathbf{L}_I^c \tag{3.58}$$

This is the fundamental equation of attitude dynamics. It is important to note that this result holds even if the center of mass undergoes acceleration, as it usually does. Equation (3.58) only holds in a non-rotating frame, however.[4]

The separation into contributions from center-of-mass motion and motion about the center of mass also holds for the kinetic energy. We have

$$\begin{aligned}E_k^0 &\equiv \frac{1}{2}\sum_{i=1}^{n} m_i \|\mathbf{v}^{i0}\|^2 = \frac{1}{2}\sum_{i=1}^{n} m_i (\mathbf{v}^{ic} + \mathbf{v}^{c0}) \cdot (\mathbf{v}^{ic} + \mathbf{v}^{c0}) \\ &= \frac{1}{2}\sum_{i=1}^{n} m_i \|\mathbf{v}^{ic}\|^2 + \frac{1}{2} M \|\mathbf{v}^{c0}\|^2 = E_k^c + \frac{1}{2} M \|\mathbf{v}^{c0}\|^2 \end{aligned} \tag{3.59}$$

The derivative of the kinetic energy is

$$\dot{E}_k^0 = \sum_{i=1}^{n} m_i \mathbf{v}_I^{i0} \cdot \dot{\mathbf{v}}_I^{i0} = \sum_{i=1}^{n} (\mathbf{v}_I^{ic} + \mathbf{v}_I^{c0}) \cdot \mathbf{F}_I^i = \sum_{i=1}^{n} \mathbf{v}_I^{ic} \cdot \mathbf{F}_I^i + \mathbf{v}_I^{c0} \cdot \mathbf{F}_I \tag{3.60}$$

The internal forces cancel in the $\mathbf{v}_I^{c0} \cdot \mathbf{F}_I^i$ sum due to the *weak* form of Newton's third law of motion, i.e. this cancelation does not require the force between two mass points to be along the line joining them. The internal forces do not cancel in

[4] This is discussed in Sect. 2.6.2.

the other term, though. This means that internal forces cannot affect the energy of center-of-mass motion, but they can modify the energy of rotation about the center of mass. It is apparent that the last term of Eq. (3.60) is equal to the derivative of the last term of Eq. (3.59), from which it follows that

$$\dot{E}_k^c = \sum_{i=1}^{n} \mathbf{v}_I^{ic} \cdot \mathbf{F}_I^i \tag{3.61}$$

3.3.2 Rigid Body Dynamics

A rigid body is defined by the existence of a reference frame, called the *body frame* B in which all the vectors $\mathbf{r}_B^{ic}$ are constant. The body frame is not unique; any frame related to it by a constant orthogonal transformation is also a body frame. The constancy of the vectors in the body frame and Eq. (3.14) allow us to obtain the velocity of a mass point in the inertial frame as

$$\mathbf{v}_I^{ic} = \dot{\mathbf{r}}_I^{ic} = A_{IB}\dot{\mathbf{r}}_B^{ic} - \boldsymbol{\omega}_I^{IB} \times \mathbf{r}_I^{ic} = \boldsymbol{\omega}_I^{BI} \times \mathbf{r}_I^{ic} \tag{3.62}$$

where we have used Eq. (3.8) to obtain the last form. Substituting this into Eq. (3.56) gives

$$\mathbf{H}_I^c = \sum_{i=1}^{n} m_i \mathbf{r}_I^{ic} \times \mathbf{v}_I^{ic} = \sum_{i=1}^{n} m_i \mathbf{r}_I^{ic} \times (\boldsymbol{\omega}_I^{BI} \times \mathbf{r}_I^{ic}) = -\sum_{i=1}^{n} m_i [\mathbf{r}_I^{ic}\times]^2 \boldsymbol{\omega}_I^{BI} = J_I^c\, \boldsymbol{\omega}_I^{BI} \tag{3.63}$$

The last equality defines the representation in the frame I of the symmetric 3×3 matrix J_I^c known as the *moment of inertia tensor*, or MOI.[5] The MOI in Eq. (3.63) is specific to frame I, but we can define it in a general frame by

$$J^c \equiv -\sum_{i=1}^{n} m_i [\mathbf{r}^{ic}\times]^2 = \sum_{i=1}^{n} m_i \left[\|\mathbf{r}^{ic}\|^2 I_3 - \mathbf{r}^{ic}(\mathbf{r}^{ic})^T\right] \tag{3.64}$$

which defines the MOI in the frame in which the vectors $\mathbf{r}^{ic}$ are represented, whatever that frame is. In fact the MOI is almost always expressed in the body frame

$$J_B^c = -\sum_{i=1}^{n} m_i [\mathbf{r}_B^{ic}\times]^2 = \sum_{i=1}^{n} m_i \left[\|\mathbf{r}_B^{ic}\|^2 I_3 - \mathbf{r}_B^{ic}(\mathbf{r}_B^{ic})^T\right] \tag{3.65}$$

[5] The MOI is more specifically a *second-rank tensor*, which means that it transforms by Eq. (2.52) under reference frame transformations. This follows directly from the fact that $\mathbf{r}_B^{ic} = A_{BI}\mathbf{r}_I^{ic}$.

because it is constant in that frame. The angular momentum in the body frame is given, using Eqs. (2.52) and (2.42), by

$$\mathbf{H}_B^c = A_{BI}\mathbf{H}_I^c = A_{BI}J_I^c\,\boldsymbol{\omega}_I^{BI} = A_{BI}J_I^c A_{BI}^T A_{BI}\boldsymbol{\omega}_I^{BI} = J_B^c\,\boldsymbol{\omega}_B^{BI}. \tag{3.66}$$

The *parallel axis theorem* can be used to find the MOI of a rigid body about an arbitrary point p in terms of its MOI about its center of mass:

$$\begin{aligned} J^p &= \sum_{i=1}^{n} m_i \left[\|\mathbf{r}^{ip}\|^2 I_3 - \mathbf{r}^{ip}(\mathbf{r}^{ip})^T\right] \\ &= \sum_{i=1}^{n} m_i \left[\|(\mathbf{r}^{ic} + \mathbf{r}^{cp})\|^2 I_3 - (\mathbf{r}^{ic} + \mathbf{r}^{cp})(\mathbf{r}^{ic} + \mathbf{r}^{cp})^T\right] \\ &= M\left[\|\mathbf{r}^{cp}\|^2 I_3 - \mathbf{r}^{cp}(\mathbf{r}^{cp})^T\right] + J^c \end{aligned} \tag{3.67}$$

with Eq. (3.55) causing the other terms in the sum to vanish. This allows us to express the MOI of a large body in terms of the MOIs of m subassemblies as

$$J^c = \sum_{k=1}^{m} \left\{M_k\left[\|\mathbf{r}^{c_k c}\|^2 I_3 - \mathbf{r}^{c_k c}(\mathbf{r}^{c_k c})^T\right] + J^{c_k}\right\} \tag{3.68}$$

where c is the center of mass of the whole system and M_k, c_k, and J^{c_k} denote the mass, location of the center of mass, and MOI about c_k of the kth subassembly. This is the method used to compute MOIs in practice, where the subassemblies can be structural elements, electronics boxes, reaction wheel assemblies, star trackers, etc. The MOIs of the subassemblies can be directly measured or they can be computed by breaking the subassemblies down into sub-subassemblies.

The matrix elements of the MOI tensor are given explicitly by

$$[J^c]_{11} = \sum_{i=1}^{n} m_i \left[(r_2^{ic})^2 + (r_3^{ic})^2\right] \tag{3.69a}$$

$$[J^c]_{22} = \sum_{i=1}^{n} m_i \left[(r_3^{ic})^2 + (r_1^{ic})^2\right] \tag{3.69b}$$

$$[J^c]_{33} = \sum_{i=1}^{n} m_i \left[(r_1^{ic})^2 + (r_2^{ic})^2\right] \tag{3.69c}$$

$$[J^c]_{k\ell} = -\sum_{i=1}^{n} m_i\, r_k^{ic}\, r_\ell^{ic}, \quad \text{for} \quad k \neq \ell \tag{3.69d}$$

The off-diagonal elements, $[J^c]_{k\ell}$, or their negatives, $-[J^c]_{k\ell}$, are often referred to as the *products of inertia*.[6]

Being a real symmetric 3×3 matrix, the MOI tensor has three orthogonal eigenvectors $\mathbf{e}_B^k$ and three real eigenvalues J_k satisfying the relation

$$J_B^c \mathbf{e}_B^k = J_k \mathbf{e}_B^k, \quad \text{for} \quad k = 1, 2, 3 \tag{3.70}$$

The unit vectors $\mathbf{e}_B^k$ are called the *principal axes* and the scalars J_k are known as the *principal moments of inertia*. The transformation of the MOI tensor from an arbitrary body frame to the principal axis frame is given by

$$A_{BP}^T J_B^c A_{BP} = J_P^c = \text{diag}\left([J_1 \; J_2 \; J_3]\right) \tag{3.71}$$

where $A_{BP} = [\mathbf{e}_B^1 \; \mathbf{e}_B^2 \; \mathbf{e}_B^3]$. In the principal axis frame Eq. (3.69) has the form

$$J_1 = \sum_{i=1}^{n} m_i \left[(r_{P2}^{ic})^2 + (r_{P3}^{ic})^2\right] \tag{3.72a}$$

$$J_2 = \sum_{i=1}^{n} m_i \left[(r_{P3}^{ic})^2 + (r_{P1}^{ic})^2\right] \tag{3.72b}$$

$$J_3 = \sum_{i=1}^{n} m_i \left[(r_{P1}^{ic})^2 + (r_{P2}^{ic})^2\right] \tag{3.72c}$$

$$0 = \sum_{i=1}^{n} m_i \, r_{Pk}^{ic} \, r_{P\ell}^{ic}, \quad \text{for} \quad k \neq \ell \tag{3.72d}$$

The sum in the last of these equations must have balancing positive and negative contributions, expressing the intuitive idea that the mass is distributed symmetrically about the principal axes. In particular, any axis of rotational symmetry of a mass distribution is a principal axis. The first three equations show that the principal moments are all positive, unless the mass is all concentrated on a mathematical straight line, which is impossible for a real physical body. It can also be seen from these equations that the principal moments of inertia satisfy the triangle inequalities

$$J_k \leq J_\ell + J_m \tag{3.73}$$

where equality holds only if all the mass is concentrated in the $\ell - m$ plane, and where k, ℓ, and m are any permutation of the indices $1, 2, 3$.

[6]Be warned that notation varies. The majority of authors use I for the MOI, but we reserve this notation for the identity matrix. Some denote our J_{kk} by I_{kk} and our $J_{k\ell}$ for $k \neq \ell$ by $-I_{k\ell}$, but this unfortunate notation should be shunned.

It also follows from this analysis that the MOI tensor of any real physical body has an inverse in any body frame, and we can write Eq. (3.66) as

$$\boldsymbol{\omega}_B^{BI} = (J_B^c)^{-1}\mathbf{H}_B^c \tag{3.74}$$

Implicit in Eqs. (3.66) and (3.74) is the key fact that the angular momentum and angular velocity of a rigid body are parallel if and only if the body rotates about a principal axis.

The rotational kinetic energy of a rigid body can also be expressed in terms of the MOI tensor. Substituting Eq. (3.62) into Eq. (3.59) gives

$$\begin{aligned} E_k^c &= \frac{1}{2}\sum_{i=1}^{n} m_i \|\mathbf{v}^{ic}\|^2 = \frac{1}{2}\sum_{i=1}^{n} m_i (\boldsymbol{\omega}_I^{BI} \times \mathbf{r}_I^{ic})^T (\boldsymbol{\omega}_I^{BI} \times \mathbf{r}_I^{ic}) \\ &= \frac{1}{2}\sum_{i=1}^{n} m_i \left([\mathbf{r}_I^{ic}\times]\boldsymbol{\omega}_I^{BI}\right)^T \left([\mathbf{r}_I^{ic}\times]\boldsymbol{\omega}_I^{BI}\right) = \frac{1}{2}(\boldsymbol{\omega}_I^{BI})^T J_I^c\, \boldsymbol{\omega}_I^{BI} \end{aligned} \tag{3.75}$$

The rotational kinetic energy can be computed in any frame F by

$$E_k^c = \frac{1}{2}(\boldsymbol{\omega}_F^{BI})^T J_F^c\, \boldsymbol{\omega}_F^{BI} = \frac{1}{2}\boldsymbol{\omega}_F^{BI} \cdot \mathbf{H}_F^c = \frac{1}{2}(\mathbf{H}_F^c)^T (J_F^c)^{-1}\, \mathbf{H}_F^c \tag{3.76}$$

The time derivative of Eq. (3.75) is, with Eqs. (3.63) and (3.58),

$$\dot{E}_k^c = (\boldsymbol{\omega}_I^{BI})^T J_I^c\, \dot{\boldsymbol{\omega}}_I^{BI} = \boldsymbol{\omega}_I^{BI} \cdot \mathbf{L}_I^c = \boldsymbol{\omega}_B^{BI} \cdot \mathbf{L}_B^c \tag{3.77}$$

showing that only external torques can modify the energy of rotation of a *rigid* body about its center of mass. This can be seen more explicitly by substituting Eq. (3.62) into Eq. (3.61), giving

$$\dot{E}_k^c = \sum_{i=1}^{n} (\boldsymbol{\omega}_I^{BI} \times \mathbf{r}_I^{ic}) \cdot \left(\sum_{j=1}^{n} \mathbf{F}_I^{ij} + \mathbf{F}_I^{iext} \right) = \boldsymbol{\omega}_I^{BI} \cdot \mathbf{L}_I^c \tag{3.78}$$

The sum over the internal forces $\mathbf{F}_I^{ij}$ vanishes for the same reason that the corresponding sum in Eq. (3.52) gave zero contribution, and the final equality follows from applying Eqs. (2.56a) and (3.57).

We can now collect in one place the basic equations needed to model the attitude motion of a rigid body. We will assume that the attitude is parameterized by a quaternion, but any other representation could be used instead:

$$\dot{\mathbf{H}}_I^c = \mathbf{L}_I^c \tag{3.79a}$$

$$\mathbf{H}_B^c = A(\mathbf{q}_{BI})\mathbf{H}_I^c \tag{3.79b}$$

$$\boldsymbol{\omega}_B^{BI} = (J_B^c)^{-1}\mathbf{H}_B^c \tag{3.79c}$$

$$\dot{\mathbf{q}}_{BI} = \frac{1}{2}\boldsymbol{\omega}_B^{BI} \otimes \mathbf{q}_{BI} \tag{3.79d}$$

The external torques are often more easily computed in the body frame, so Eq. (3.14) is often employed to replace the first two of these equations by

$$\dot{\mathbf{H}}_B^c = \mathbf{L}_B^c - \boldsymbol{\omega}_B^{BI} \times \mathbf{H}_B^c \tag{3.80}$$

A further reduction in the number of equations can be achieved by combining the above equation with Eq. (3.66) to obtain *Euler's rotational equation*

$$\dot{\boldsymbol{\omega}}_B^{BI} = (J_B^c)^{-1}\left[\mathbf{L}_B^c - \boldsymbol{\omega}_B^{BI} \times (J_B^c\,\boldsymbol{\omega}_B^{BI})\right] \tag{3.81}$$

This equation and a kinematics equation, such as the quaternion kinematics equation, provide a complete description of the motion of a rigid body.

Use of the principal axis reference frame is generally not especially advantageous for numerical integration of the equations of motion, since a computer can easily deal with a full 3×3 inertia tensor. The principal axis frame is almost invariably employed for analytical studies of attitude motion, however, and we will use it in the next subsection.

3.3.3 Rigid Body Motion

We now begin a discussion of the motion produced by the rigid body dynamic and kinematic equations. This section will consider the qualitative aspects of the motion, without solving the kinematic and dynamic differential equations explicitly. Then Sect. 3.3.4 will discuss in detail the solutions in the absence of torques. We will simplify the notation by omitting the superscript c, with the understanding that we always treat motion with respect to the center of mass unless explicitly indicated otherwise. We will denote the components of $\mathbf{H}_B$ in a principal axis frame by H_1, H_2, H_3 and the components of $\boldsymbol{\omega}_B^{BI}$ by $\omega_1, \omega_2, \omega_3$. There are many discussions of rigid body motion in the literature, including notable ones by Goldstein [10], Kaplan [17], Markley [20], and Hughes [14].

3.3.3.1 Spin Stabilization

Equation (3.58) tells us that $\mathbf{H}_I$ is constant if there are no external torques. This has led to the technique of *spin stabilization* of spacecraft. The basic idea is to stabilize the pointing direction of one axis by spinning the spacecraft about that axis.

If a torque of magnitude L transverse to the direction of the spin angular momentum acts on a spinning spacecraft, the change in angular momentum over a time interval Δt will be

$$\|\Delta \mathbf{H}_I\| = L\Delta t \approx H\Delta\vartheta \tag{3.82}$$

where H is the magnitude of the angular momentum and $\Delta\vartheta$ is the angle (measured in radians) over which it rotates. It is clear that a larger amount of angular momentum will result in a smaller angular motion for a given level of disturbance torque. Spin stabilization was widely employed early in the space program, then was largely displaced by active control methods, but has made a comeback in the era of microsatellites and nanosatellites.

It is important for spin stabilization that the angular momentum also have a constant direction in the body frame. Equation (3.80) says that this will be the case if $\boldsymbol{\omega}_B^{BI} \times \mathbf{H}_B = \mathbf{0}$, which requires the rotation axis to be a principal axis of the inertia tensor. Thus we want the spacecraft to rotate about a principal axis. If the spacecraft spins about a principal axis, but this does not align precisely with the desired pointing axis, *coning* results, with the pointing axis rotating at the spin rate around a cone centered on the inertially fixed angular momentum. The only way to eliminate coning is to carefully balance the spacecraft. This is generally accomplished by adding balance weights before launch similar to balancing an automobile tire, but some spacecraft have carried movable weights into orbit to allow compensation for inertia shifts caused by launch forces or to provide better balance than can be measured on the ground.

If the angular momentum is not perfectly aligned with a principal axis of inertia, the angular momentum will not be constant in the body frame. The resulting motion of the angular momentum, and of the angular velocity, is called *nutation*.[7] For torque-free motion, $\|\mathbf{H}_B\| = \|\mathbf{H}_I\| \equiv H$ is constant during nutation, so the angular momentum vector moves on the surface of a sphere of radius H in the body frame.

Investigating the stability of the motion for angular velocity close to, but not exactly on, a principal axis shows that all principal axes are not created equal for the purpose of spin stabilization. We will see that spin stabilization should always be about the principal axis with the largest or smallest principal moment of inertia, known as the *major* or *minor* principal axis, respectively, with a strong preference for the major principal axis. If there are no torques, the component form of Eq. (3.80) in the principal axis frame is

$$\dot{H}_1 = (J_3^{-1} - J_2^{-1})\, H_2\, H_3 = [(J_2 - J_3)/(J_2 J_3)]\, H_2\, H_3 \tag{3.83a}$$

$$\dot{H}_2 = (J_1^{-1} - J_3^{-1})\, H_3\, H_1 = [(J_3 - J_1)/(J_3 J_1)]\, H_3\, H_1 \tag{3.83b}$$

$$\dot{H}_3 = (J_2^{-1} - J_1^{-1})\, H_1\, H_2 = [(J_1 - J_2)/(J_1 J_2)]\, H_1\, H_2 \tag{3.83c}$$

[7] This is the usual aerospace meaning of the term *nutation*; it is used quite differently in other applications of classical mechanics to refer to a wobbling or nodding motion.

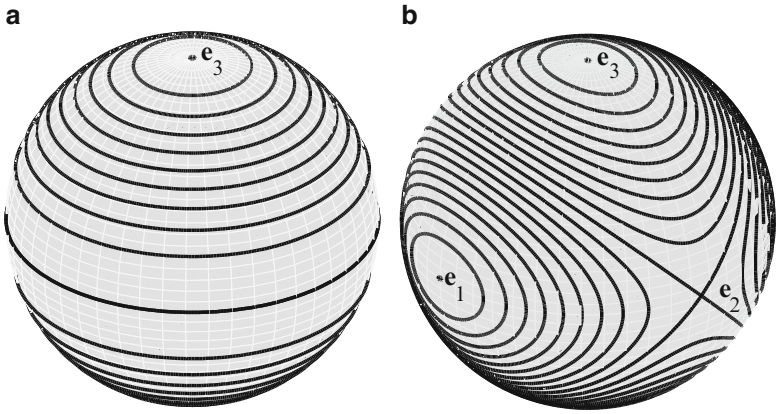

Fig. 3.2 Constant energy paths on the angular momentum sphere. (**a**) Axisymmetric inertia ratios $J_1 : J_2 : J_3 = 4 : 4 : 6$. (**b**) Triaxial inertia ratios $J_1 : J_2 : J_3 = 3 : 4 : 6$

We will choose the spin axis to be close to the $\mathbf{e}_3$ axis for the purpose of the following argument, which means that H_1 and H_2 are both much less than H_3. Thus their product on the right side of Eq. (3.83c) is negligibly small, and we can approximate H_3 as being constant. Then differentiating Eq. (3.83a) and substituting Eq. (3.83b) gives

$$\ddot{H}_1(t) = [(J_2 - J_3)(J_3 - J_1)/(J_1 J_2)](H_3/J_3)^2 H_1(t) \tag{3.84}$$

If J_3 is the largest or smallest principal moment, the product $(J_2 - J_3)(J_3 - J_1)$ is negative, resulting in a periodic motion of H_1. Then Eq. (3.83a) shows that H_2 also undergoes periodic motion with the same period. This is nutation about the $\mathbf{e}_3$ axis. The product $(J_2 - J_3)(J_3 - J_1)$ is positive if J_3 is intermediate between J_1 and J_2, however, and H_1 and H_2 both grow exponentially.[8] Thus rotation about an intermediate principal axis is inherently unstable. It is also possible that J_3 is equal to one of the other principal moments. If $J_3 = J_1$, for instance, then Eq. (3.83b) tells us that H_2 is exactly constant, and Eq. (3.83a) says that H_1 grows linearly with time. This motion is also unstable, although not exponentially unstable.

This behavior is illustrated in Fig. 3.2a,b, which show the torque-free motion of $\mathbf{H}_B$ on the sphere of radius H for two different inertia tensors. The rotational kinetic energy in a principal axis frame is given by

$$2E_k = H_1^2/J_1 + H_2^2/J_2 + H_3^2/J_3 \tag{3.85}$$

[8] Exponential growth continues until the right side of Eq. (3.83c) is no longer negligible.

For a given angular momentum magnitude, the kinetic energy is restricted to the range

$$H^2/J_{\max} \leq 2E_k \leq H^2/J_{\min} \tag{3.86}$$

where $J_{\min}$ and $J_{\max}$ are the minimum and maximum principal moments of inertia. Conservation of energy confines the motion of $\mathbf{H}_B$ to a path on the sphere and Fig. 3.2a,b show these paths for energy levels with even spacing $0.025H^2/J_{\max}$ in the range allowed by Eq. (3.86).

We will first discuss the simpler axially symmetric, or *axisymmetric* case, with two principal moments equal. We will take $\mathbf{e}_3$ to be the axis of symmetry of the inertia tensor in this case, which is shown in Fig. 3.2a. The axes $\mathbf{e}_1$ and $\mathbf{e}_2$ are not shown on the figure because they can be any two axes in the equatorial plane that form a right-handed orthogonal triad with $\mathbf{e}_3$. With $J_1 = J_2 \equiv J_t$, where the subscript t denotes "transverse," Eq. (3.85) becomes

$$2E_k = (H_1^2 + H_2^2)/J_t + H_3^2/J_3 \tag{3.87}$$

It follows that

$$H_3 = \pm\left[\frac{J_3(H^2 - 2J_t E_k)}{J_3 - J_t}\right]^{1/2} \tag{3.88a}$$

$$H_t \equiv \left[H_1^2 + H_2^2\right]^{1/2} = \left[\frac{J_t(2J_3 E_k - H^2)}{J_3 - J_t}\right]^{1/2} \tag{3.88b}$$

This shows that nutation of an axisymmetric body is motion of the angular momentum vector in the body frame along circles of constant radius H_t a constant distance of H_3 above or below the equatorial plane, as shown in Fig. 3.2a. This extends the analysis of Eq. (3.84) to nutation with any allowable magnitude about the major or minor principal axis $\pm\mathbf{e}_3$. The figure also shows that there are no small nutation paths close to the $\mathbf{e}_1 - \mathbf{e}_2$ plane.

Figure 3.2b illustrates the *triaxial* case, where no two principal moments are equal. We have labeled the principal axes for this discussion so that $J_1 < J_2 < J_3$. The paths followed by nutational motion about the major and minor axes are not simple circles in this case; their exact form will be found in Sect. 3.3.4. We see that there is no stable motion about the intermediate axis $\pm\mathbf{e}_2$ in this case. Instead, we find motion along two great circles passing through $\mathbf{e}_2$. They are called *separatrices*, because they separate nutational motion about $\pm\mathbf{e}_1$ from nutational motion about $\pm\mathbf{e}_3$. The separatrices are the curves for $2E_k = H^2/J_2$, so they satisfy the equation

$$(H_3^2 + H_2^2 + H_1^2)/J_2 = H_1^2/J_1 + H_2^2/J_2 + H_3^2/J_3 \tag{3.89}$$

which gives

$$\frac{H_3}{H_1} = \left[\frac{J_3(J_2 - J_1)}{J_1(J_3 - J_2)}\right]^{1/2} \tag{3.90}$$

Fig. 3.3 William Pickering, James Van Allen, and Wernher von Braun holding a Full-Scale Model of Explorer 1. Source: NASA

3.3.3.2 Energy Dissipation

We have seen that stable rotation is possible around either a major or minor principal axis of inertia. However, internal forces in a body that is not completely rigid can lead to energy dissipation. If external torques are absent, $\mathbf{H}_I$ will be constant, but the rotational energy will decrease to its minimum value of $H^2/J_{\max}$, resulting in stable rotation about a major principal axis. If the intended spin axis is a minor axis, energy dissipation will result in *flat spin*, an undesirable rotation about an axis perpendicular to the preferred axis. A famous example of this is the pencil-shaped Explorer 1, the first Earth satellite successfully launched by the United States, which was intended to spin about its longitudinal axis. Its entry into flat spin was attributed to energy dissipation in the flexible turnstile antenna array, comprising the four wires attached to the fuselage just aft of Wernher von Braun's right hand in Fig. 3.3 [5].

Steady spin about the major principal axis is commonly the desired outcome, with spin-stabilized spacecraft designed to be more nearly disc-shaped than pencil-shaped; and passive *nutation dampers* are often placed on these spacecraft to produce this result. For triaxial inertia, energy dissipation can result in motion starting with increasing nutation about $\pm\mathbf{e}_1$, then crossing one of the separatrices, followed by decreasing nutation about either $\mathbf{e}_3$ or $-\mathbf{e}_3$, depending on where a separatrix is crossed. Because $\mathbf{H}_I$ is fixed in the inertial frame, these two outcomes result in the pointing axis being oriented in opposite directions in inertial space. It is usually the case that only one of these pointing directions is satisfactory, which requires careful control of the energy damping to ensure the correct crossing of the separatrix.

3.3.3.3 Poinsot's Construction

The discussion up to this point has not provided a picture of the motion in the inertial frame. *Poinsot's construction* supplies this picture by focusing on angular velocity rather than angular momentum [10, 14, 17]. Conservation of energy in torque-free motion restricts angular velocity to the surface of the *inertia ellipsoid* defined by

$$2E_k = (\boldsymbol{\omega}_B^{BI})^T J_B \boldsymbol{\omega}_B^{BI} = J_1\omega_1^2 + J_2\omega_2^2 + J_3\omega_3^2 \tag{3.91}$$

with semimajor axes of length $\sqrt{2E_k/J_1}$, $\sqrt{2E_k/J_2}$, $\sqrt{2E_k/J_3}$. A small change $\Delta\boldsymbol{\omega}$ in the angular velocity would result in an energy change

$$\Delta E_k = (\boldsymbol{\omega}_B^{BI})^T J_B^c \, \Delta\boldsymbol{\omega} = \mathbf{H}_B \cdot \Delta\boldsymbol{\omega} \tag{3.92}$$

which is zero if $\Delta\boldsymbol{\omega}$ is perpendicular to the angular momentum. Changes $\Delta\boldsymbol{\omega}$ that do not change E_k are in the plane tangent to the inertia ellipsoid, leading to the conclusion that the normal to the inertia ellipsoid at any $\boldsymbol{\omega}_B^{BI}$ is in the direction of the angular momentum $\mathbf{H}_B = J_B\boldsymbol{\omega}_B^{BI}$.

Each closed path on the momentum sphere illustrated in Fig. 3.2a or b maps onto a closed path called a *polhode* on the inertia ellipsoid. As the angular velocity moves along the polhode, the inertia ellipsoid (which is fixed in the rigid body) moves in such away that the normal to its surface at the position of the instantaneous angular velocity maintains a fixed direction (that of $\mathbf{H}_I$) in inertial space. But Poinsot tells us more. Writing the energy equation in the form $2E_k = \boldsymbol{\omega}_I^{BI} \cdot \mathbf{H}_I$ reveals that the component of $\boldsymbol{\omega}_I^{BI}$ parallel to $\mathbf{H}_I$ has the constant value $2E_k/H$. Thus the tip of the vector $\boldsymbol{\omega}_I^{BI}$ always lies in a fixed plane normal to $\mathbf{H}_I$ at a distance of $2E_k/H$ from the center of the inertia ellipsoid. The path followed by the angular velocity in this *invariant plane* is called the *herpolhode*. Thus the inertia ellipsoid rolls on the invariant plane with its center at a fixed point a distance $2E_k/H$ above the plane and with the tip of the angular velocity vector as the point of contact. Since the angular velocity is the instantaneous axis of rotation, there is no slippage at the contact point, and Poinsot's construction can be succinctly summarized by the statement that the polhode rolls without slipping on the herpolhode lying in the invariant plane.[9] Goldstein [10], Kaplan [17], and Hughes [14] have pictures illustrating Poinsot's construction.

Poinsot's construction is not especially easy to visualize, and there is a simpler picture for the familiar axial symmetry case. In any case, we now turn to analytic solutions of the equations of motion, which are often more useful than pictures for estimation and control applications.

[9] A statement aptly characterized by Goldstein [10] as "jabberwockian."

3.3.4 Torque-Free Motion of a Rigid Body

Analytic solutions of the rigid body equations of motion are customarily expressed in terms of angular velocity rather than angular momentum. Thus we will consider the component form of Eq. (3.81) in the principal axis frame in the absence of torques:

$$\dot{\omega}_1(t) = [(J_2 - J_3)/J_1]\,\omega_2(t)\,\omega_3(t) \tag{3.93a}$$

$$\dot{\omega}_2(t) = [(J_3 - J_1)/J_2]\,\omega_3(t)\,\omega_1(t) \tag{3.93b}$$

$$\dot{\omega}_3(t) = [(J_1 - J_2)/J_3]\,\omega_1(t)\,\omega_2(t) \tag{3.93c}$$

As we saw in Sect. 3.3.3, the rate of rotation about one of the principal axes is constant if the moments of inertia about the other two principal axes are equal. We will treat this simpler case of axial symmetry first, and then turn to the case of a triaxial inertia tensor.

3.3.4.1 Axial Symmetry

Taking $\mathbf{e}_3$ to be the axis of symmetry of the inertia tensor, we have

$$\dot{\omega}_1(t) = (1 - J_3/J_t)\,\omega_2(t)\,\omega_3(t) \tag{3.94a}$$

$$\dot{\omega}_2(t) = -(1 - J_3/J_t)\,\omega_3(t)\,\omega_1(t) \tag{3.94b}$$

$$\dot{\omega}_3(t) = 0 \tag{3.94c}$$

This means that ω_3 is constant, so we can omit the time argument. Note that ω_3 is exactly constant for axial symmetry, as opposed to its approximate constancy in the stability analysis of Sect. 3.3.3. It follows from Eq. (3.88a) that

$$\omega_3 = \frac{H_3}{J_3} = \pm\left[\frac{H^2 - 2J_t E_k}{J_3(J_3 - J_t)}\right]^{1/2} \tag{3.95}$$

Differentiating Eq. (3.94a) and substituting Eq. (3.94b) gives

$$\ddot{\omega}_1(t) = -(1 - J_3/J_t)^2\omega_3^2\,\omega_1(t) \tag{3.96}$$

which has the solution

$$\omega_1(t) = \omega_t \sin(\psi_0 + \omega_p t) \tag{3.97}$$

where ψ_0 is a constant initial phase,

$$\omega_p \equiv (1 - J_3/J_t)\omega_3 \tag{3.98}$$

and, from Eq. (3.88b),

$$\omega_t = \frac{H_t}{J_t} = \left[\frac{2J_3E_k - H^2}{J_t(J_3 - J_t)}\right]^{1/2} \tag{3.99}$$

Then $\omega_2(t)$ is given by Eq. (3.94a) as

$$\omega_2(t) = \omega_t \cos(\psi_0 + \omega_p t) \tag{3.100}$$

The angular rate ω_p is called the *body nutation rate* because it is the rate at which the angular velocity vector rotates about the symmetry axis in the body frame. Note that ω_p has the same sign as ω_3 if $J_t > J_3$ and the opposite sign if $J_t < J_3$. If $J_t = J_3$, there is no nutation, only steady rotation, since all axes are principal axes in that case. The angular momentum rotates about the symmetry axis in the body frame at the same rate, because the three vectors $\mathbf{H}, \boldsymbol{\omega}$, and $\mathbf{e}_3$ are coplanar in the case of triaxial symmetry, as is easily seen from the relation

$$\mathbf{H} = J_t \begin{bmatrix} \omega_1 \\ \omega_2 \\ 0 \end{bmatrix} + J_3 \begin{bmatrix} 0 \\ 0 \\ \omega_3 \end{bmatrix} = J_t\boldsymbol{\omega} + (J_3 - J_t)\omega_3\mathbf{e}_3 \tag{3.101}$$

The speed at which the angular momentum vector moves over the sphere of radius H in the body frame can also be computed by

$$\|\dot{\mathbf{H}}_B\|^2 = \|\boldsymbol{\omega}_B^{BI} \times \mathbf{H}_B\|^2 = H^2\|\boldsymbol{\omega}_B^{BI}\|^2 - (\boldsymbol{\omega}_B^{BI} \cdot \mathbf{H}_B)^2 = H^2\|\boldsymbol{\omega}_B^{BI}\|^2 - (2E_k)^2 \tag{3.102}$$

Substituting Eqs. (3.95), (3.99), (3.97) and (3.100) and performing some straightforward algebra gives

$$\|\dot{\mathbf{H}}_B\| = |(J_3 - J_t)\omega_t\omega_3| = H_t|\omega_p| \tag{3.103}$$

It is easy to see that these equations give $\|\dot{\mathbf{H}}_B\| = 0$ for rotation about a principal axis, for which either ω_t or ω_3 is zero.

By using the addition formulas for the sine and cosine, we can express the transverse components of the angular velocity in terms of their initial values:

$$\omega_1(t) = \omega_{01}\cos\omega_p t + \omega_{02}\sin\omega_p t \tag{3.104a}$$

$$\omega_2(t) = \omega_{02}\cos\omega_p t - \omega_{01}\sin\omega_p t \tag{3.104b}$$

where $\omega_{01} = \omega_t \sin\psi_0$ and $\omega_{02} = \omega_t \cos\psi_0$.

We must now solve the kinematic equations of motion in order to have a complete mathematical description of the torque-free motion. We will follow the almost universal practice for torque-free motion of specifying the attitude by 3−1−3 Euler angles. This gives us three first-order equations to integrate, which would lead to

three constants of integration in addition to the three we have already found: H, E_k, and ψ_0. Two of these constants can be thought of as specifying the fixed direction of $\mathbf{H}_I$, and we eliminate these by choosing the inertial reference frame with its third axis in the direction of $\mathbf{H}_I$. Then the angular momentum in the body frame is given by

$$\mathbf{H}_B = \begin{bmatrix} J_t\omega_1 \\ J_t\omega_2 \\ J_3\omega_3 \end{bmatrix} = A_{BI}\mathbf{H}_I = A_{313}(\phi,\theta,\psi)\begin{bmatrix} 0 \\ 0 \\ H \end{bmatrix} = H\begin{bmatrix} \sin\psi\sin\theta \\ \cos\psi\sin\theta \\ \cos\theta \end{bmatrix} \tag{3.105}$$

where Eq. (2.162) provides the last equality. We immediately see that the *nutation angle* θ has constant value between 0 and π given by

$$\theta = \cos^{-1}(J_3\,\omega_3/H) \tag{3.106}$$

and comparison of the first two components of Eq. (3.105) with Eqs. (3.97) and (3.100) shows that

$$\sin\theta = J_t\,\omega_t/H \geq 0 \tag{3.107}$$

and

$$\psi = \psi_0 + \omega_p t \tag{3.108}$$

up to an irrelevant multiple of 2π. This explains our choice of the notation ψ_0 in Eq. (3.97). The third Euler angle is found by integrating Eq. (3.38) using Eq. (3.42):

$$\dot{\phi} = \csc\theta(\omega_1\sin\psi + \omega_2\cos\psi) = \omega_t\csc\theta = H/J_t \equiv \omega_\ell \tag{3.109}$$

so that

$$\phi = \phi_0 + \omega_\ell t \tag{3.110}$$

The angular rate ω_ℓ is called the *inertial nutation rate* because it is the rate at which the angular velocity vector and the symmetry axis of the rigid body rotate about the fixed angular momentum vector in the inertial frame. Equation (3.98) can be used to write Eq. (3.101) as

$$\boldsymbol{\omega} = \mathbf{H}/J_t + (1 - J_3/J_t)\omega_3\mathbf{e}_3 = \mathbf{H}/J_t + \omega_p\mathbf{e}_3 \tag{3.111}$$

This shows that the angular velocity in the axisymmetric case can be expressed as the sum of two (nonorthogonal) vectors of magnitude ω_ℓ and ω_p.

We complete the analysis of axisymmetric motion by finding the components of the angular velocity in the inertial frame. These are given by

$$\boldsymbol{\omega}_I^{BI} = A_{IB}\boldsymbol{\omega}_B^{BI} = A_{313}^T(\phi,\theta,\psi)\begin{bmatrix}\omega_1\\ \omega_2\\ \omega_3\end{bmatrix}$$

$$= A(\mathbf{e}_3,-\phi)A(\mathbf{e}_1,-\theta)A(\mathbf{e}_3,-\psi)\begin{bmatrix}\omega_t\sin\psi\\ \omega_t\cos\psi\\ \omega_3\end{bmatrix} \tag{3.112}$$

Performing the matrix multiplications and applying Eqs. (2.108), (3.106), and (3.107) gives

$$A(\mathbf{e}_1,-\theta)A(\mathbf{e}_3,-\psi)\begin{bmatrix}\omega_t\sin\psi\\ \omega_t\cos\psi\\ \omega_3\end{bmatrix} = A(\mathbf{e}_1,-\theta)\begin{bmatrix}0\\ \omega_t\\ \omega_3\end{bmatrix}$$

$$= \begin{bmatrix}0\\ \omega_t\cos\theta-\omega_3\sin\theta\\ \omega_3\cos\theta+\omega_t\sin\theta\end{bmatrix} = \frac{1}{H}\begin{bmatrix}0\\ (J_3-J_t)\omega_t\omega_3\\ 2E_k\end{bmatrix} \tag{3.113}$$

Thus the component of $\boldsymbol{\omega}_I^{BI}$ parallel to $\mathbf{H}_I$ has the constant value $2E_k/H$, as we saw in our discussion of Poinsot's construction; and the component transverse to $\mathbf{H}_I$ has a magnitude agreeing with Eq. (3.103) and rotates around a circular herpolhode at the inertial nutation rate.

We now present a pictorial view of this motion, which is the specialization of Poinsot's construction to the axisymmetric case. The angular velocity vector precesses at rate ω_ℓ and at an angle θ from the angular momentum vector around a *space cone* fixed in the inertial frame. At the same time, the angular velocity vector precesses at rate ω_p and at an angle β from the $\mathbf{e}_3$ axis around a *body cone* fixed in the body frame. These cones are illustrated in Fig. 3.4a for the prolate case and in Fig. 3.4b for the oblate case.[10] The cones are tangent at the angular velocity because $\mathbf{H}$, $\boldsymbol{\omega}$, and $\mathbf{e}_3$ are coplanar, and there is no slippage along the line of tangency because that is the axis around which the rotation takes place. Thus, as viewed from the inertial frame, the body cone (and the spacecraft which is fixed to it) rolls without slipping around the fixed space cone; while, as viewed from the body frame, the space cone (and the universe which is fixed to it) rolls without slipping around the fixed body cone.

The body cone angle β obeys

$$\cos\beta = \omega_3/\|\boldsymbol{\omega}\| \quad \text{and} \quad \sin\beta = \omega_t/\|\boldsymbol{\omega}\| \tag{3.114}$$

[10]The figure illustrates the case of $\omega_3 > 0$, but a corresponding figure for $\omega_3 < 0$ shows that all the discussion of this section holds in that case also.

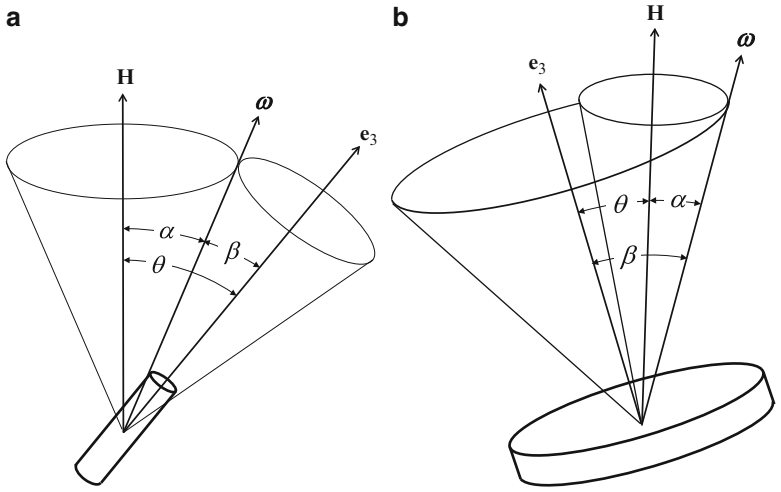

Fig. 3.4 Torque-free motion of an axisymmetric rigid body. (**a**) Prolate rigid body $J_3 < J_t$. (**b**) Oblate rigid body $J_3 > J_t$

and comparison with Eqs. (3.106) and (3.107) shows that the space cone rolls on the outside of the body cone for a prolate rigid body and on the inside for an oblate body, as shown in the figure. This explains why ω_p has the same sign as ω_3 in the prolate case and the opposite sign in the oblate case, in agreement with Eq. (3.98). Finally, we note from the figure that α, the angle between $\mathbf{H}$ and $\boldsymbol{\omega}$, is equal to $|\theta - \beta|$. This relation can be verified algebraically by applying Eqs. (3.106), (3.107) and (3.114) to get

$$H\|\boldsymbol{\omega}\|(\cos\beta\cos\theta + \sin\beta\sin\theta) = 2E_k = \mathbf{H}\cdot\boldsymbol{\omega} = H\|\boldsymbol{\omega}\|\cos\alpha \tag{3.115}$$

3.3.4.2 Triaxial Symmetry

We will designate the intermediate principal moment of inertia by J_2 in the triaxial case. We saw in the discussion of Fig. 3.2b that the separatrices divide the motion into two regimes. For $2E_k < H^2/J_2$ the motion has the form of nutation about the principal axis having the largest moment of inertia, and $2E_k > H^2/J_2$ results in nutation about the principal axis with the smallest moment of inertia. Motion along a separatrix is a limiting case of either of these regimes. In order that one analytic formulation will cover both of these cases, we label the principal axes so that nutation is always about $\pm\mathbf{e}_3$. Thus

$$J_1 < J_2 < J_3 \quad \text{if} \quad 2E_k \le H^2/J_2, \tag{3.116a}$$

$$J_1 > J_2 > J_3 \quad \text{if} \quad 2E_k \ge H^2/J_2 \tag{3.116b}$$

No component of the angular velocity is constant in the triaxial symmetry case, so the solutions cannot be expressed in terms of sines and cosines. The closed-form solutions are expressed in terms of the Jacobian elliptic functions [1] $\mathrm{sn}(u|m)$, $\mathrm{cn}(u|m)$, and $\mathrm{dn}(u|m)$ with *argument* u and *parameter* m.[11] We define two signs, s_1 and s_3 equal to ± 1, a dimensionless constant

$$\kappa \equiv \left[\frac{J_1(J_3 - J_1)}{J_2(J_3 - J_2)}\right]^{1/2} \tag{3.117}$$

and the angular rates

$$\omega_{1m} \equiv \left[\frac{2J_3E_k - H^2}{J_1(J_3 - J_1)}\right]^{1/2} \tag{3.118a}$$

$$\omega_{3m} \equiv \left[\frac{H^2 - 2J_1E_k}{J_3(J_3 - J_1)}\right]^{1/2} \tag{3.118b}$$

Then

$$\omega_1(t) = s_1\,\omega_{1m}\,\mathrm{cn}\left(u_0 + \omega_p t\,|m\right) \tag{3.119a}$$

$$\omega_2(t) = -s_1\kappa\,\omega_{1m}\,\mathrm{sn}\left(u_0 + \omega_p t\,|m\right) \tag{3.119b}$$

$$\omega_3(t) = s_3\,\omega_{3m}\,\mathrm{dn}\left(u_0 + \omega_p t\,|m\right) \tag{3.119c}$$

where

$$\omega_p = [(J_2 - J_3)/J_1]\kappa s_3\,\omega_{3m} \tag{3.120}$$

and

$$m = \frac{(J_2 - J_1)(2J_3E_k - H^2)}{(J_3 - J_2)(H^2 - 2J_1E_k)} \tag{3.121}$$

Note that $m = 0$ for $2E_k = H^2/J_3$, $m = 1$ for $2E_k = H^2/J_2$, and Eq. (3.116) restricts m to always lie between these limits. Figure 3.5a shows the Jacobian elliptic functions for $m = 0.7$, which is the value for $2J_2E_k = (16/17)H^2$ with the inertia ratios used in Fig. 3.2b.

The Jacobian elliptic functions obey the differential equations

$$\mathrm{sn}'(u|m) = \mathrm{cn}(u|m)\mathrm{dn}(u|m) \tag{3.122a}$$

$$\mathrm{cn}'(u|m) = -\mathrm{sn}(u|m)\mathrm{dn}(u|m) \tag{3.122b}$$

$$\mathrm{dn}'(u|m) = -m\,\mathrm{sn}(u|m)\mathrm{cn}(u|m) \tag{3.122c}$$

[11] Some authors, including Hughes [14], use the *modulus* $k \equiv m^{1/2}$ in place of the parameter.

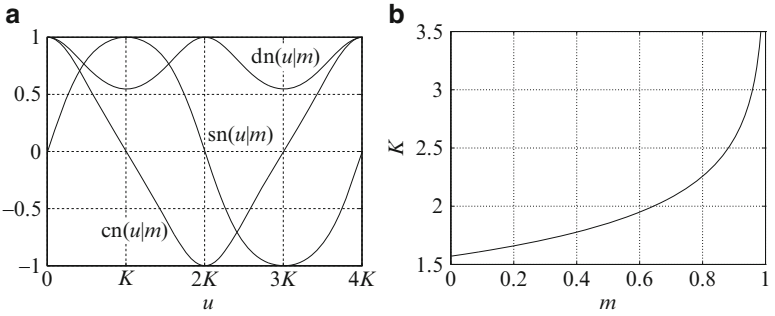

Fig. 3.5 Jacobian elliptic functions. (**a**) Elliptic functions for $m = 0.7$. (**b**) Dependence of the quarter-period K on m

where the prime denotes differentiation with respect to the argument. These equations can be used to show that Eq. (3.119) obeys Eq. (3.93). The Jacobian elliptic functions also satisfy the quadratic relations

$$\mathrm{cn}^2(u|m) + \mathrm{sn}^2(u|m) = \mathrm{dn}^2(u|m) + m\,\mathrm{sn}^2(u|m) = 1, \tag{3.123}$$

which verify that E_k and H are the rotational kinetic energy and angular momentum magnitude, respectively, of the solutions. The Jacobian elliptic functions are related to the usual trigonometric functions by

$$\mathrm{sn}(u|m) = \sin\varphi \tag{3.124a}$$

$$\mathrm{cn}(u|m) = \cos\varphi \tag{3.124b}$$

$$\mathrm{dn}(u|m) = (1 - m\sin^2\varphi)^{1/2} \tag{3.124c}$$

where φ is an implicit function of u and m defined by the integral relation

$$u = \int_0^{\varphi} \frac{d\theta}{(1 - m\sin^2\theta)^{1/2}} \tag{3.125}$$

These equations lead directly to Eqs. (3.122) and (3.123). The quarter-period of the sine or cosine function is $\pi/2$, so the quarter-period of the Jacobian elliptic functions is

$$K(m) = \int_0^{\pi/2} \frac{d\theta}{(1 - m\sin^2\theta)^{1/2}} \tag{3.126}$$

This integral is known as a *complete elliptic integral of the first kind* [1]. Figure 3.5b shows that the quarter-period is an increasing function of m, equal to $\pi/2$ for $m = 0$ and becoming infinite as m goes to 1.

We can use the addition formulas for the Jacobian elliptic functions to write the triaxial solutions in terms of initial values. The addition formulas are, with the parameter m omitted for notational convenience,

$$\mathrm{sn}(u+v) = \frac{\mathrm{sn}u\,\mathrm{cn}v\,\mathrm{dn}v + \mathrm{sn}v\,\mathrm{cn}u\,\mathrm{dn}u}{1 - m\,\mathrm{sn}^2u\,\mathrm{sn}^2v} \tag{3.127a}$$

$$\mathrm{cn}(u+v) = \frac{\mathrm{cn}u\,\mathrm{cn}v - \mathrm{sn}u\,\mathrm{dn}u\,\mathrm{sn}v\,\mathrm{dn}v}{1 - m\,\mathrm{sn}^2u\,\mathrm{sn}^2v} \tag{3.127b}$$

$$\mathrm{dn}(u+v) = \frac{\mathrm{dn}u\,\mathrm{dn}v - m\,\mathrm{sn}u\,\mathrm{cn}u\,\mathrm{sn}v\,\mathrm{cn}v}{1 - m\,\mathrm{sn}^2u\,\mathrm{sn}^2v} \tag{3.127c}$$

The angular rates can then be written in terms of the initial values as

$$\omega_1(t) = \frac{\omega_{01}\,\mathrm{cn}(\omega_p t) + [(J_2 - J_3)/J_1](\omega_{02}\omega_{03}/\omega_p)\mathrm{sn}(\omega_p t)\mathrm{dn}(\omega_p t)}{1 - [(J_2 - J_3)/J_1][(J_1 - J_2)/J_3](\omega_{02}/\omega_p)^2\mathrm{sn}^2(\omega_p t)} \tag{3.128a}$$

$$\omega_2(t) = \frac{\omega_{02}\,\mathrm{cn}(\omega_p t)\mathrm{dn}(\omega_p t) + [(J_3 - J_1)/J_2](\omega_{03}\omega_{01}/\omega_p)\mathrm{sn}(\omega_p t)}{1 - [(J_2 - J_3)/J_1][(J_1 - J_2)/J_3](\omega_{02}/\omega_p)^2\mathrm{sn}^2(\omega_p t)} \tag{3.128b}$$

$$\omega_3(t) = \frac{\omega_{03}\,\mathrm{dn}(\omega_p t) + [(J_1 - J_2)/J_3](\omega_{01}\omega_{02}/\omega_p)\mathrm{sn}(\omega_p t)\mathrm{cn}(\omega_p t)}{1 - [(J_2 - J_3)/J_1][(J_1 - J_2)/J_3](\omega_{02}/\omega_p)^2\mathrm{sn}^2(\omega_p t)} \tag{3.128c}$$

Comparison with Eq. (3.93) suggests the alternative form

$$\omega_1(t) = \frac{\omega_{01}\,\mathrm{cn}(\omega_p t) + (\dot\omega_{01}/\omega_p)\mathrm{sn}(\omega_p t)\mathrm{dn}(\omega_p t)}{1 - \omega_p^{-2}(\dot\omega_{01}/\omega_{03})(\dot\omega_{03}/\omega_{01})\mathrm{sn}^2(\omega_p t)} \tag{3.129a}$$

$$\omega_2(t) = \frac{\omega_{02}\,\mathrm{cn}(\omega_p t)\mathrm{dn}(\omega_p t) + (\dot\omega_{02}/\omega_p)\mathrm{sn}(\omega_p t)}{1 - \omega_p^{-2}(\dot\omega_{01}/\omega_{03})(\dot\omega_{03}/\omega_{01})\mathrm{sn}^2(\omega_p t)} \tag{3.129b}$$

$$\omega_3(t) = \frac{\omega_{03}\,\mathrm{dn}(\omega_p t) + (\dot\omega_{03}/\omega_p)\mathrm{sn}(\omega_p t)\mathrm{cn}(\omega_p t)}{1 - \omega_p^{-2}(\dot\omega_{01}/\omega_{03})(\dot\omega_{03}/\omega_{01})\mathrm{sn}^2(\omega_p t)} \tag{3.129c}$$

but neither form is especially convenient for computation.

Equations (3.124) and (3.125) show that the Jacobian elliptic functions are equal to the usual trigonometric functions for $m = 0$:

$$\mathrm{sn}(u|0) = \sin u \tag{3.130a}$$

$$\mathrm{cn}(u|0) = \cos u \tag{3.130b}$$

$$\mathrm{dn}(u|0) = 1 \tag{3.130c}$$

They are equal to hyperbolic functions for $m = 1$:

$$\mathrm{sn}(u|1) = \tanh u \tag{3.131a}$$

$$\mathrm{cn}(u|1) = \mathrm{sech}\, u \tag{3.131b}$$

$$\mathrm{dn}(u|1) = \mathrm{sech}\, u \tag{3.131c}$$

which give the solution for motion on the separatrices with $2E_k = H^2/J_2$. These solutions are not periodic, because the quarter-period is infinite for $m = 1$; they approach pure rotation about the principal axis $\mathbf{e}_2$ in the infinite past and future.

The speed at which the angular momentum vector moves over the sphere of radius H in the body frame is also given by Eq. (3.102) in the triaxial case, but substituting Eq. (3.119) shows that the speed is not constant in this case. However, nice expressions can be found for the maximum and minimum speeds. The maximum, reached when $\omega_2 = 0$ or equivalently where the path of the angular momentum crosses the plane perpendicular to $\mathbf{e}_2$, is

$$\|\dot{\mathbf{H}}_B\|_{\max} = (J_3 - J_1)\omega_{1m}\omega_{3m} \tag{3.132}$$

The minimum, reached when $|\omega_2|$ obtains its maximum value on the path, is

$$\|\dot{\mathbf{H}}_B\|^2_{\min} = (H^2 - 2J_2E_k)(2J_3E_k - H^2)/(J_2J_3) \tag{3.133}$$

The maximum speed has the same form as for an axisymmetric body, but the minimum speed is specific to the triaxial case. It is not difficult to see that these equations give $\|\dot{\mathbf{H}}_B\| = 0$ for rotation about a principal axis, for which $2E_k = H^2/J_k$.

Solution of the kinematic equations proceeds in parallel with the axisymmetric case. We again specify the attitude by $3-1-3$ Euler angles and choose the inertial reference frame with its third axis in the direction of $\mathbf{H}_I$. Then Eq. (3.105) holds, and substituting Eq. (3.119) gives

$$\begin{bmatrix} J_1\,\omega_1 \\ J_2\,\omega_2 \\ J_3\,\omega_3 \end{bmatrix} = \begin{bmatrix} s_1 J_1\,\omega_{1m}\,\mathrm{cn}\left(u_0 + \omega_p t\,|m\right) \\ -s_1 J_2 \kappa\,\omega_{1m}\,\mathrm{sn}\left(u_0 + \omega_p t\,|m\right) \\ s_3 J_3\,\omega_{3m}\,\mathrm{dn}\left(u_0 + \omega_p t\,|m\right) \end{bmatrix} = H \begin{bmatrix} \sin\psi\,\sin\theta \\ \cos\psi\,\sin\theta \\ \cos\theta \end{bmatrix} \tag{3.134}$$

Thus

$$\cos\theta = (s_3 J_3\,\omega_{3m}/H)\mathrm{dn}\left(u_0 + \omega_p t\,|m\right) \tag{3.135a}$$

$$\psi = \mathrm{atan2}\left(s_1 J_1 \mathrm{cn}\left(u_0 + \omega_p t\,|m\right), -s_1 J_2 \kappa\,\mathrm{sn}\left(u_0 + \omega_p t\,|m\right)\right) \tag{3.135b}$$

The third Euler angle is found by integrating Eq. (3.38) using Eq. (3.42):

$$\begin{aligned} \dot{\phi} &= \csc\theta(\omega_1 \sin\psi + \omega_2 \cos\psi) = H\,\frac{J_1\omega_1^2 + J_2\omega_2^2}{J_1^2\omega_1^2 + J_2^2\omega_2^2} \\ &= H\,\frac{J_3 - J_2 + (J_2 - J_1)\mathrm{sn}^2(u_0 + \omega_p t\,|m)}{J_1(J_3 - J_2) + J_3(J_2 - J_1)\mathrm{sn}^2(u_0 + \omega_p t\,|m)} \end{aligned} \tag{3.136}$$

The quantities θ, $\dot{\psi}$, and $\dot{\phi}$ are all time-varying for triaxial inertia.

We complete the analysis of motion for triaxial inertia by finding the components of the angular velocity in the inertial frame. These are given by Eq. (3.112). Performing the matrix multiplications gives

$$A(\mathbf{e}_1,-\theta)A(\mathbf{e}_3,-\psi)\begin{bmatrix}\omega_1\\ \omega_2\\ \omega_3\end{bmatrix} = A(\mathbf{e}_1,-\theta)\begin{bmatrix}(J_2-J_1)\,\omega_1\omega_2/(H\sin\theta)\\ (J_1\omega_1^2+J_2\omega_2^2)/(H\sin\theta)\\ \omega_3\end{bmatrix}$$

$$= \frac{1}{H}\begin{bmatrix}(J_2-J_1)\,\omega_1\omega_2\csc\theta\\ (J_1^2\omega_1^2+J_2^2\omega_2^2)^{-1/2}J_1(J_3-J_1)\omega_{1m}^2\omega_3\\ 2E_k\end{bmatrix} \tag{3.137}$$

The component of $\boldsymbol{\omega}_I^{BI}$ parallel to $\mathbf{H}_I$ has the constant value $2E_k/H$, as required by Poinsot's construction and as we saw for axial symmetry. The component of $\boldsymbol{\omega}_I^{BI}$ transverse to $\mathbf{H}_I$ has a varying magnitude, so the herpolhode is not a circle. In fact, the herpolhode is not a closed curve in general, because the motion of ϕ is not commensurate with that of θ and ψ.

It is not difficult to see that all the equations for the triaxial case reduce to the axisymmetric results, with $\psi_0 = (u_0 + s_1\pi/2)$, if $J_1 = J_2$.

3.3.5 *Internal Torques*

Although some spacecraft can be modeled as a single rigid body, many are more complex. These complexities can be of several types. The first is that the spacecraft consists of a number of rigid bodies connected by joints having one, two, or three degrees of rotational freedom, and sometimes admitting sliding motion as well. Powerful and general commercial software packages, many employing Kane's method [15, 16] are available to analyze the dynamics of these systems. We will only treat the simple cases of reaction wheels and control moment gyros, the more complex systems being beyond the scope of this text.

The rigid model of a spacecraft will also be inadequate if we cannot ignore flexibility, which is always present at some level. Analysis of flexible body dynamics generally uses finite element methods [30], which are almost always applied to the analysis of large spacecraft but are also beyond the scope of this text.

A third complication often encountered is fluid motion, or *slosh* of liquid fuels or cryogens. We will only give a basic introduction to the treatment of slosh, with references to the literature.

These internal torques are also known as *momentum exchange* torques because they result in, or are a result of, the exchange of angular momentum between components of complex spacecraft without a change in the net system momentum of the entire spacecraft. As the listing above indicates, some internal torques constitute undesirable disturbances, while others are provided by control mechanisms.

3.3.5.1 Reaction Wheels and Control Moment Gyros

Let us consider a spacecraft with n reaction wheels or control moment gyros, labeled by an index ℓ. Each wheel rotates about its spin axis with an angular velocity ω_ℓ^w with respect to the body. The wheel is axially symmetric about its spin axis, so the spin axis is a principal axis with principal moment of inertia $J_\ell^{\parallel}$, and every axis perpendicular to the spin axis is a principal axis with moment $J_\ell^{\perp}$.[12] Thus the inertia tensor of the ℓth wheel in the body reference frame is

$$J_\ell^w = J_\ell^{\perp}(I_3 - \mathbf{w}_\ell \mathbf{w}_\ell^T) + J_\ell^{\parallel} \mathbf{w}_\ell \mathbf{w}_\ell^T \tag{3.138}$$

where the unit vector $\mathbf{w}_\ell$ defines the spin axis in the body frame. Letting $\tilde{J}_B$ represent the moment of inertia of the spacecraft *without* the wheels, the body frame representation of total angular momentum with respect to inertial space of the spacecraft with its wheels is

$$\begin{aligned} \mathbf{H}_B &= \tilde{J}_B \boldsymbol{\omega}_B^{BI} + \sum_{\ell=1}^{n} J_\ell^w (\boldsymbol{\omega}_B^{BI} + \omega_\ell^w \mathbf{w}_\ell) \\ &= J_B \boldsymbol{\omega}_B^{BI} + \mathbf{H}_B^w \end{aligned} \tag{3.139}$$

where

$$J_B \equiv \tilde{J}_B + \sum_{\ell=1}^{n} J_\ell^{\perp}(I_3 - \mathbf{w}_\ell \mathbf{w}_\ell^T) \tag{3.140}$$

and

$$\mathbf{H}_B^w = \sum_{\ell=1}^{n} J_\ell^{\parallel}(\mathbf{w}_\ell \cdot \boldsymbol{\omega}_B^{BI} + \omega_\ell^w)\mathbf{w}_\ell \equiv \sum_{\ell=1}^{n} H_\ell^w \mathbf{w}_\ell \tag{3.141}$$

The body moment of inertia J_B is defined to include the inertia of the wheels transverse to their spin axes, but not their inertia along their spin axes. Note that $\mathbf{H}_B^w$ denotes only the angular momentum of the wheels along their spin axes; the momentum of their transverse rotation is included in $J_B \boldsymbol{\omega}_B^{BI}$. The difference between reaction wheels and control moment gyros is that $\mathbf{w}_\ell$ is fixed and ω_ℓ^w is changing for reaction wheels, while ω_ℓ^w is constant and $\mathbf{w}_\ell$ is moved by a gimbal (or gimbals) for control moment gyros. Some control wheels have been designed to vary both $\mathbf{w}_\ell$ and ω_ℓ^w, but these have not been widely employed.

[12] This describes an ideal wheel. The effects of deviations from this ideal case will be discussed in Sect. 4.8.

The rotational dynamics of the spacecraft with wheels are still described by Eq. (3.80) but with Eq. (3.79c) replaced by

$$\boldsymbol{\omega}_B^{BI} = J_B^{-1}(\mathbf{H}_B - \mathbf{H}_B^w) \tag{3.142}$$

where the superscript c is understood but has been omitted for economy of notation. For many attitude determination problems, $\boldsymbol{\omega}_B^{BI}$ and $\mathbf{H}_B^w$ can be computed from Eqs. (3.141) and (3.142) using tachometer data for reaction wheels or axis orientation data for control moment gyros.[13] To complete the dynamics analysis, however, a dynamic equation for $\mathbf{H}_B^w$ is required.

The rotational kinetic energy of a spacecraft with reaction wheels or control moment gyros is given by

$$\begin{aligned} E_k &= \frac{1}{2}(\boldsymbol{\omega}_B^{BI})^T \tilde{J}_B\, \boldsymbol{\omega}_B^{BI} + \frac{1}{2}\sum_{\ell=1}^{n}(\boldsymbol{\omega}_B^{BI} + \omega_\ell^w \mathbf{w}_\ell)^T J_\ell^w (\boldsymbol{\omega}_B^{BI} + \omega_\ell^w \mathbf{w}_\ell) \\ &= \frac{1}{2}(\boldsymbol{\omega}_B^{BI})^T J_B\, \boldsymbol{\omega}_B^{BI} + \frac{1}{2}\sum_{\ell=1}^{n} J_\ell^{\parallel}(\mathbf{w}_\ell \cdot \boldsymbol{\omega}_B^{BI} + \omega_\ell^w)^2 \\ &= \frac{1}{2}(\boldsymbol{\omega}_B^{BI})^T J_B\, \boldsymbol{\omega}_B^{BI} + \frac{1}{2}\sum_{\ell=1}^{n}(J_\ell^{\parallel})^{-1}(H_\ell^w)^2 \end{aligned} \tag{3.143}$$

Now let us specialize to reaction wheels, which have been more commonly employed in small to medium size spacecraft than control moment gyros. The representations in the body frame of the angular momenta of the wheels are the terms in the sum in Eq. (3.139). It follows that the equation of motion of the ℓth wheel in the body frame, using Eq. (3.138), is

$$\begin{aligned} J_\ell^w(\dot{\boldsymbol{\omega}}_B^{BI} + \dot{\omega}_\ell^w \mathbf{w}_\ell) &= \tilde{\mathbf{L}}_\ell^w - \boldsymbol{\omega}_B^{BI} \times [J_\ell^w(\boldsymbol{\omega}_B^{BI} + \omega_\ell^w \mathbf{w}_\ell)] \\ &= \tilde{\mathbf{L}}_\ell^w + [\, J_\ell^{\perp}(\mathbf{w}_\ell \cdot \boldsymbol{\omega}_B^{BI}) - H_\ell^w](\boldsymbol{\omega}_B^{BI} \times \mathbf{w}_\ell) \end{aligned} \tag{3.144}$$

where $\tilde{\mathbf{L}}_\ell^w$ is the applied torque. The other term on the right side of this equation is perpendicular to the spin axis; it is provided by the wheel bearings and is not under our direct control. Thus we are only interested in the spin axis component of the torque, which is denoted by L_ℓ^w and is given by

$$L_\ell^w = \mathbf{w}_\ell^T J_\ell^w(\dot{\boldsymbol{\omega}}_B^{BI} + \dot{\omega}_\ell^w \mathbf{w}_\ell) = J_\ell^{\parallel}(\mathbf{w}_\ell \cdot \dot{\boldsymbol{\omega}}_B^{BI} + \dot{\omega}_\ell^w) = \dot{H}_\ell^w \tag{3.145}$$

Then Eq. (3.141) gives[14]

[13] Giving $\boldsymbol{\omega}_B^{BI} = (J_B + \sum_{\ell=1}^n J_\ell^{\parallel}\mathbf{w}_\ell\mathbf{w}_\ell^T)^{-1}(\mathbf{H}_B - \sum_{\ell=1}^n J_\ell^{\parallel}\omega_\ell^w\mathbf{w}_\ell)$ and $\mathbf{H}_B^w = \mathbf{H}_B - J_B\boldsymbol{\omega}_B^{BI}$.

[14] Including an $\boldsymbol{\omega}_B^{BI} \times \mathbf{H}_B^w$ term in this equation would be double-counting, because this term was already accounted for in Eq. (3.144). It can be seen explicitly in Eq. (3.147).

$$\dot{\mathbf{H}}_B^w = \sum_{\ell=1}^{n} \dot{H}_\ell^w \mathbf{w}_\ell = \sum_{\ell=1}^{n} L_\ell^w \mathbf{w}_\ell \equiv \mathbf{L}_B^w \tag{3.146}$$

We find the generalization of Eq. (3.81) to include reaction wheels by substituting this and Eq. (3.139) into Eq. (3.80), yielding

$$\dot{\boldsymbol{\omega}}_B^{BI} = J_B^{-1}[\mathbf{L}_B - \mathbf{L}_B^w - \boldsymbol{\omega}_B^{BI} \times (J_B \boldsymbol{\omega}_B^{BI} + \mathbf{H}_B^w)] \tag{3.147}$$

The negative sign before $\mathbf{L}_B^w$ on the right side reflects Newton's third law of motion.

The rate of change of the kinetic energy is given by the derivative of Eq. (3.143),

$$\begin{aligned} \dot{E}_k &= \boldsymbol{\omega}_B^{BI} \cdot [\mathbf{L}_B - \mathbf{L}_B^w - \boldsymbol{\omega}_B^{BI} \times \mathbf{H}_B] + \sum_{\ell=1}^{n} (\mathbf{w}_\ell \cdot \boldsymbol{\omega}_B^{BI} + \omega_\ell^w) L_\ell^w \\ &= \boldsymbol{\omega}_B^{BI} \cdot \mathbf{L}_B + \sum_{\ell=1}^{n} \omega_\ell^w L_\ell^w \end{aligned} \tag{3.148}$$

This shows that the change in rotational kinetic energy is the sum of work done by the external torques and by the internal torques, a concrete illustration of the observation made near the end of Sect. 3.3.1 that internal forces can modify the energy of rotational motion.

3.3.5.2 Slosh

Spacecraft often contain fluids, the most common being propellants or cryogens for cooling scientific instruments. The motion of these fluids, commonly called *slosh*, is often a source of undesirable attitude disturbances. Slosh is very difficult to analyze, and we will only provide a very brief introduction to some of the issues; the monograph by Dodge provides a much more thorough discussion [8].

Fuel slosh can be a major problem for spin-stabilized spacecraft. In particular, the energy dissipated by sloshing liquid can destabilize the motion of a spacecraft spinning about an axis of minimum MOI, as discussed in Sect. 3.3.3.2. Slosh is also a problem for repointing maneuvers of fine-pointing spacecraft. A strong coupling of the fluid motion to the rigid spacecraft can cause large pointing errors. Weak coupling of the fluid motion, on the other hand, leads to smaller pointing errors, but the perturbations take a correspondingly longer time to damp out. The resulting long resettling times after attitude maneuvers decrease the time available for fine-pointing observations.

The main dynamic effects of slosh result from the motion of the center of mass of the moving fluid. This is usually represented by the mechanical model of a pendulum or a mass on a spring to represent the motion of the fluid, along with some mechanism to provide damping. Dodge presents methods for computing the frequencies and damping coefficients for fluid containers of various shapes, including a variety of baffles, diaphragms, and fluid management devices. The *fill factor* of the container, the ratio of the amount of fluid contained to the capacity of

the full tank, is a critical factor. Slosh is much less of a factor for a nearly full tank, because the center of mass cannot move much, or for a nearly empty tank, because there is less moving mass.

Fluid motion in microgravity is different from motion under acceleration forces. The relative importance of inertia forces, gravity forces, and capillary forces on fluid motion are characterized by the *Bond number*, the *Weber number*, and the *Froude number*, while the *Reynolds number* determines the importance of viscosity. All these considerations are important for providing a slosh model from first principles, but it is quite common for the parameters in a slosh model to be determined empirically.

3.3.6 External Torques

External torques involve an interaction with entities external to the spacecraft. As opposed to internal torques, external torques change the overall momentum of the spacecraft. In common with internal torques, external torques include both undesirable disturbance torques and torques deliberately applied for control.

3.3.6.1 Gravity-Gradient Torque

Any nonsymmetrical rigid body in a gravity field is subject to a gravity-gradient torque. We compute this torque by summing the contributions of the gravitational forces on the various point masses constituting the rigid body as in Eq. (3.57). The gravitational force on the ith particle is

$$\mathbf{F}^{iext} = m_i \mathbf{g}(\mathbf{r}^{i0}) = m_i \left. \nabla_{\mathbf{r}} U(\mathbf{r}) \right|_{\mathbf{r}=\mathbf{r}^{i0}} \tag{3.149}$$

where $U(\mathbf{r})$ is the gravity potential.[15] Assuming that only first-order variations in the gravitational field over the rigid body are significant allows us to expand in a power series, retaining only the first two terms:

$$\mathbf{F}^{iext} = m_i \mathbf{g}(\mathbf{r}^{ic} + \mathbf{r}^{c0}) = m_i [\mathbf{g}(\mathbf{r}^{c0}) + G(\mathbf{r}^{c0})\mathbf{r}^{ic}] \tag{3.150}$$

where

$$G(\mathbf{r}^{c0}) \equiv \left. \frac{\partial \mathbf{g}(\mathbf{r})}{\partial \mathbf{r}} \right|_{\mathbf{r}=\mathbf{r}^{c0}} = \left. \frac{\partial^2 U(\mathbf{r})}{\partial \mathbf{r}\, \partial \mathbf{r}^T} \right|_{\mathbf{r}=\mathbf{r}^{c0}} \tag{3.151}$$

[15] As is customary in astrodynamics, this is the *negative* of the potential energy.

is the gravity-gradient tensor, evaluated at the center of mass. It follows from Eq. (3.151) that the gravity-gradient tensor is a symmetric 3×3 matrix.

Substituting into Eq. (3.57) gives the gravity-gradient torque about the center of mass as

$$\begin{aligned}\mathbf{L}_{gg}^{c} &= \sum_{i=1}^{n} m_i \mathbf{r}^{ic} \times \left[\mathbf{g}(\mathbf{r}^{c0}) + G(\mathbf{r}^{c0})\mathbf{r}^{ic}\right] \\ &= \left(\sum_{i=1}^{n} m_i \mathbf{r}^{ic}\right) \times \mathbf{g}(\mathbf{r}^{c0}) + \sum_{i=1}^{n} m_i \mathbf{r}^{ic} \times \left[G(\mathbf{r}^{c0})\mathbf{r}^{ic}\right] \\ &= \sum_{i=1}^{n} m_i \mathbf{r}^{ic} \times \left[G(\mathbf{r}^{c0})\mathbf{r}^{ic}\right] \end{aligned} \tag{3.152}$$

using the property of the center of mass expressed in Eq. (3.55).

It is usually adequate to approximate the gravity field as spherically symmetric for computing gravity-gradient torques. In this case, we have

$$\mathbf{g}(\mathbf{r}) = -\frac{\mu \mathbf{r}}{r^3} \tag{3.153}$$

and therefore

$$G(\mathbf{r}) = -\frac{\mu}{r^3}\left(I_3 - 3\frac{\mathbf{r}\mathbf{r}^T}{r^2}\right) \tag{3.154}$$

where μ is the gravitational parameter of the central body, the product of its mass and Newton's universal gravitational constant, $\mathbf{r}$ is the radius vector from the center of the central body, and $r \equiv \|\mathbf{r}\|$. Inserting this into Eq. (3.152), letting $\mathbf{r}^{c0} = -r\mathbf{n}$, where $\mathbf{n}$ is the body frame representation of a nadir-pointing unit vector, and using various identities for dot and cross products gives

$$\begin{aligned}\mathbf{L}_{gg}^{c} &= -\frac{\mu}{r^3}\sum_{i=1}^{n} m_i \mathbf{r}^{ic} \times \left(\mathbf{r}^{ic} - 3\mathbf{n}\mathbf{n}^T\mathbf{r}^{ic}\right) = -\frac{3\mu}{r^3}\mathbf{n} \times \sum_{i=1}^{n} m_i (\mathbf{r}^{ic})(\mathbf{r}^{ic})^T\mathbf{n} \\ &= \frac{3\mu}{r^3}\mathbf{n} \times \sum_{i=1}^{n} m_i \left[\|\mathbf{r}^{ic}\|^2 I_3 - (\mathbf{r}^{ic})(\mathbf{r}^{ic})^T\right]\mathbf{n} = \frac{3\mu}{r^3}\mathbf{n} \times (J^c\mathbf{n}) \end{aligned} \tag{3.155}$$

where J^c is the moment of inertia tensor about the center of mass. Several properties of the gravity-gradient torque are apparent from this equation: its magnitude is inversely proportional to the cube of the distance from the center of the central body, its direction is perpendicular to the radius vector from the central body, and it vanishes if the radius vector is along any principal axis of inertia.

To investigate the gravity-gradient torque in more detail, consider a spacecraft orbiting the Earth (or any celestial body) and oriented to the nadir. We represent the

attitude relative to the LVLH frame[16] by a 3–2–1 Euler angle sequence of yaw $= \phi$, pitch $= \theta$, and roll $= \psi$ angles. The nadir vector is the $\mathbf{e}_3$ axis in the LVLH frame, so the nadir vector in the body frame is given by Eq. (2.164) as

$$\mathbf{n} = A_{321}(\phi, \theta, \psi) \begin{bmatrix} 0 \\ 0 \\ 1 \end{bmatrix} = \begin{bmatrix} -\sin\theta \\ \cos\theta \sin\psi \\ \cos\theta \cos\psi \end{bmatrix} \tag{3.156}$$

Substituting this into Eq. (3.155) and assuming that the body frame is a principal axis frame gives

$$\mathbf{L}_{gg}^{c} = \frac{3\mu}{r^3} \begin{bmatrix} (J_3 - J_2)\cos^2\theta \cos\psi \sin\psi \\ (J_3 - J_1)\cos\theta \sin\theta \cos\psi \\ (J_1 - J_2)\cos\theta \sin\theta \sin\psi \end{bmatrix} \tag{3.157}$$

We notice that the torque does not depend on the yaw angle, which is one of the reasons for choosing a $3-2-1$ sequence to specify the attitude.[17] The yaw angle can be quite large for some missions, with 180° yaw maneuvers used to keep one side of the spacecraft cool by facing it away from the Sun. The roll and pitch angles are usually small, though, and almost certainly less than 90° in magnitude. It is clear that the gravity-gradient torque vanishes if the roll and pitch are both zero, so this is an equilibrium configuration. For small pitch and roll angles, the third (yaw) component of the gravity-gradient torque is small, so we will not be concerned with it. Comparing Eqs. (3.156) and (3.157) shows that the first (roll) component of the gravity-gradient torque will drive the roll angle toward zero if $J_3 < J_2$ and away from zero if $J_3 > J_2$. Similarly, the second (pitch) component of the gravity-gradient torque will drive the pitch angle toward zero if $J_3 < J_1$ and away from zero if $J_3 > J_1$. Thus the equilibrium at zero roll and pitch is a stable equilibrium if J_3 is the smallest principal moment, otherwise the equilibrium is unstable for rotations about one or both axes. Another way of stating this is that gravity-gradient torque will tend to align a spacecraft with its principal axis of minimum inertia aligned with the nadir vector.

Gravity-gradient torques are often used for passive stabilization of a spacecraft. A *gravity-gradient boom* with a mass at the end can be deployed along the positive or negative yaw axis to increase the J_1 and J_2 moments of inertia relative to the J_3 inertia about the desired nadir-pointing axis. The boom deployment must be carefully timed to avoid an inverted orientation, with the desired nadir-pointing axis pointing in the zenith direction. Pendular motions, known as *libration*, can be damped out by energy-dissipating *libration dampers*, which are very similar in design and function to nutation dampers. Finally, we note that the gravity-gradient torque cannot provide stability against rotations around the nadir vector. These are controlled either by active means or by employing a momentum wheel to provide a

[16] The LVLH frame is defined in Sect. 2.6.4.

[17] A $3-1-2$ sequence would serve as well.

momentum bias along the pitch axis. Issues arising from the deployment of gravity-gradient booms are described on pp. 669–677 of [19].

To handle cases more general than a spherically symmetric gravity field, we can use Eq. (2.56c) to find an expression for the gravity-gradient torque for a general gravity-gradient tensor. This identity gives, suppressing the argument of G for notational convenience,

$$\begin{aligned}[\mathbf{L}_{gg}^{c}\times] &= \sum_{i=1}^{n} m_i[(\mathbf{r}^{ic}\times G\mathbf{r}^{ic})\times] = \sum_{i=1}^{n} m_i[G\mathbf{r}^{ic}(\mathbf{r}^{ic})^T - \mathbf{r}^{ic}(G\mathbf{r}^{ic})^T] \\ &= \sum_{i=1}^{n} m_i\left[\|\mathbf{r}^{ic}\|^2 I_3 - (\mathbf{r}^{ic})(\mathbf{r}^{ic})^T\right] G^T - G\sum_{i=1}^{n} m_i\left[\|\mathbf{r}^{ic}\|^2 I_3 - (\mathbf{r}^{ic})(\mathbf{r}^{ic})^T\right] \\ &= (GJ^c)^T - GJ^c \end{aligned} \tag{3.158}$$

making use of Eq. (2.7c) and the fact that both G and J^c are symmetric.

3.3.6.2 Magnetic Torque

The torque generated by a magnetic dipole $\mathbf{m}$ in a magnetic field $\mathbf{B}$ is

$$\mathbf{L}_{\text{mag}} = \mathbf{m}\times\mathbf{B} \tag{3.159}$$

The most basic source of a magnetic dipole is a current loop. A current of I amperes flowing in a planar loop of area A produces a dipole moment of magnitude $m = IA$ in the direction normal to the plane of the loop and satisfying a right-hand rule. It follows from this definition that the natural unit for the dipole moment is Am^2. When $\mathbf{m}$ is in Am^2 and the magnetic field is specified in Tesla, Eq. (3.159) gives the torque in Nm. If there are N turns of wire in the loop, the dipole moment has magnitude $m = NIA$. The dipole moment can be significantly increased by wrapping the wire loops around a ferromagnetic core, as will be discussed in Sect. 4.10.

Magnetic control torques are used almost exclusively in near-Earth orbits, where the magnitude of the Earth's magnetic field is roughly in the range of 20–50 μT. Commercially available torquers can provide dipole moments from 1 to 1,000 Am^2, so the resulting magnetic control torques range from 2×10^{-5} to 0.05 Nm. As described in Sect. 11.1, the field strength falls off as the inverse cube of the distance from the center of the Earth, so magnetic control has rarely been employed in higher orbits, but it has sometimes been used even in geosynchronous orbits. Undesirable magnetic dipoles can lead to magnetic disturbance torques, which are generally several orders of magnitude smaller than the above estimates of control torques.

It is customary to express $\mathbf{L}_{\text{mag}}$, $\mathbf{m}$, and $\mathbf{B}$ in body-frame coordinates. There are two ways to determine the body-frame magnetic field. The first employs

measurements by an onboard three-axis magnetometer (TAM), as described in Sect. 4.5. The other method is to compute the magnetic field vector, $\mathbf{R}$, in reference-frame coordinates from a model, either a simple dipole model, the International Geomagnetic Reference Field (IGRF), or some truncated version of the IGRF, as described in Sect. 11.1. The attitude matrix then rotates the field to the body frame by $\mathbf{B} = A\mathbf{R}$. In addition to an attitude estimate, this method requires an onboard ephemeris, which in modern spacecraft would be provided by GPS, as well as an onboard magnetic field model.

One advantage of magnetic torques is that they produce no force, so they do not perturb the spacecraft's orbit. A significant disadvantage is that the torques are constrained to lie in the plane orthogonal to the magnetic field, as is clear from Eq. (3.159), so only two out of three axes can be controlled at a given time instant. However, full three-axis control is available over a complete orbit provided that the spacecraft's orbital plane does not coincide with the geomagnetic equatorial plane and does not contain the magnetic poles [3]. The Earth's rotation causes this geometry to change, so any simulation involving magnetic control should be at least 24 h in length to ensure that unfavorable magnetic field geometry does not cause a problem at some point.[18]

Because magnetic torques cannot provide three-axis control at any instant of time, they are generally employed in conjunction with some other form of attitude control. This can be passive control, such as spin stabilization [9, 11, 13, 23] or gravity-gradient stabilization [7,28,29], but it is more common to employ magnetic control in conjunction with reaction wheels. In this application, the wheels provide the actual pointing and maneuvering torques, and magnetic torques are used to unload the secular angular momentum buildup in the wheels. Reference [6] provides an analysis of the orbit-averaged behavior of magnetic control for unloading angular momentum. Some specific examples of magnetic control laws can be found in Chap. 7.

3.3.6.3 Aerodynamic Torque

For objects in low-Earth orbit, atmospheric drag is a significant source of perturbing torque. Aerodynamic torque is generally computed by modeling the spacecraft as a collection of N flat plates of area S_i and outward normal unit vector $\mathbf{n}_B^i$ expressed in the spacecraft body-fixed coordinate system. The torque depends on the velocity of the spacecraft relative to the atmosphere. This is not simply the velocity of the spacecraft in the GCI frame, because the atmosphere is not stationary in that frame. The most common assumption is that the atmosphere co-rotates with the Earth. The relative velocity in the GCI frame is then given by

$$\mathbf{v}_{\mathrm{rel}\,I} = \mathbf{v}_I + [\boldsymbol{\omega}_{\oplus I}\times]\,\mathbf{r}_I \tag{3.160}$$

[18] This point was often emphasized by Henry Hoffman of Goddard Space Flight Center.

where $\mathbf{r}_I$ and $\mathbf{v}_I$ are the position and velocity of the spacecraft expressed in the GCI coordinate frame. The Earth's angular velocity vector is $\boldsymbol{\omega}_{\oplus I} = \omega_\oplus [0 \;\; 0 \;\; 1]^T$ with $\omega_\oplus = 0.000\,072\,921\,158\,553$ rad/s. Inserting this $\boldsymbol{\omega}_{\oplus I}$ gives the relative velocity in the body frame as

$$\mathbf{v}_{\text{rel}\,B} = A \begin{bmatrix} \dot{x} + \omega_\oplus\, y \\ \dot{y} - \omega_\oplus\, x \\ \dot{z} \end{bmatrix} \tag{3.161}$$

where A is the attitude matrix. The inclination of the ith plate to the relative velocity is given by

$$\cos\theta^i_{\text{aero}} = \frac{\mathbf{n}^i_B \cdot \mathbf{v}_{\text{rel}\,B}}{\|\mathbf{v}_{\text{rel}}\|} \tag{3.162}$$

The aerodynamic force on the ith plate in the flat plate model is

$$\mathbf{F}^i_{\text{aero}} = -\frac{1}{2}\rho\, C_D \|\mathbf{v}_{\text{rel}}\| \mathbf{v}_{\text{rel}\,B}\, S_i \max\left(\cos\theta^i_{\text{aero}}, 0\right) \tag{3.163}$$

where ρ is the atmospheric density and C_D, is a dimensionless *drag coefficient*. The drag coefficient is determined empirically, and is usually in the range between 1.5 and 2.5. Methods for computing the atmospheric density are presented in Sect. 11.2.

The aerodynamic torque on the spacecraft is then

$$\mathbf{L}^i_{\text{aero}} = \sum_{i=1}^{N} \mathbf{r}^i \times \mathbf{F}^i_{\text{aero}} \tag{3.164}$$

where $\mathbf{r}^i$ is the vector from the spacecraft center of mass to the center of pressure of the ith plate. Note this algorithm does not account for potential self-shielding that would exist on concave spacecraft.

In principle, aerodynamic torques could be used for attitude control, either for passive control like the feathers on an arrow, or even for active control by providing movable surfaces. Applications of this concept have been exceedingly rare, however.

3.3.6.4 Solar Radiation Pressure Torque

Solar radiation pressure (SRP) is another source of disturbance torque. In low-Earth orbit, the effect of SRP is dominated by aerodynamics, but SRP torques will generally dominate aerodynamic torques in higher altitude orbits ($\geq$800 km). The SRP torque is zero when the spacecraft is in the shadow of the Earth or any other body, of course. In contrast to the case of aerodynamic torques, movable surfaces have been used on some spacecraft in geosynchronous orbits to balance the SRP torques. In most applications, the surfaces have been moved by daily commands, and not controlled autonomously or in real time by an onboard computer [12].

As for aerodynamic torque, we model the surface of the spacecraft as a collection of N flat plates of area S_i, outward normal $\mathbf{n}_B^i$ in the body coordinate frame, specular reflection coefficient R_{spec}^i, diffuse reflection coefficient R_{diff}^i, and absorption coefficient R_{abs}^i. Diffuse reflection is assumed to be Lambertian, which means that the intensity of the reflected light in any direction is proportional to the cosine of the angle between the reflection direction and the normal. The coefficients sum to unity; $R_{\text{spec}}^i + R_{\text{diff}}^i + R_{\text{abs}}^i = 1$.

The spacecraft-to-Sun unit vector in the body frame is

$$\mathbf{s} = A\,\mathbf{e}_{\text{sat}\odot} \tag{3.165}$$

where A is the attitude matrix and $\mathbf{e}_{\text{sat}\odot}$ is the spacecraft-to-Sun vector in the GCI frame. The angle between the Sun vector and the normal to the ith plate is given by

$$\cos\theta_{\text{SRP}}^i = \mathbf{n}_B^i \cdot \mathbf{s} \tag{3.166}$$

The SRP force on the ith plate can then be expressed as [26]

$$\mathbf{F}_{\text{SRP}} = -P_\odot S_i \left[2\left(\frac{R_{\text{diff}}^i}{3} + R_{\text{spec}}^i \cos\theta_{\text{SRP}}^i \right) \mathbf{n}_B^i + (1 - R_{\text{spec}}^i)\mathbf{s} \right] \max\left(\cos\theta_{\text{SRP}}^i, 0\right) \tag{3.167}$$

where $P_\odot$ is the solar radiation pressure. Section 11.3 present methods for computing the Sun position, solar radiation pressure, and conditions for shadowing.

The SRP torque on the spacecraft is then

$$\mathbf{L}_{\text{SRP}}^i = \sum_{i=1}^{N} \mathbf{r}^i \times \mathbf{F}_{\text{SRP}}^i \tag{3.168}$$

where $\mathbf{r}^i$ is the vector from the spacecraft center of mass to the center of pressure of the SRP on the ith plate.

This formulation has several limitations. First, the Sun is not the only source of radiation, although it is by far the largest for Earth-orbiting spacecraft. Reflected light from the Earth or the Moon, called *albedo*, can be significant if very precise dynamical modeling is required; and models incorporating this effect have been developed [4].

Secondly, the torque due to thermal radiation emitted from the spacecraft has been ignored. A spacecraft is usually in a long-term energy balance, so all the absorbed radiation is emitted as thermal radiation, although not necessarily at the same time or from the same surface as its absorption. Accurate modeling of thermal radiation requires knowledge of the absolute temperature T_i and emissivity ϵ^i (a dimensionless constant between 0 and 1) of each surface. Then the thermal radiation flux from the surface is given by the Stefan-Boltzmann law

$$\mathscr{F}_{\text{thermal}}^i = \epsilon^i \sigma T_i^4 \tag{3.169}$$

where $\sigma = 5.67 \times 10^{-8}$ Wm^{-2}K^{-4} is the Stefan-Boltzmann constant. If the thermal radiation from every surface is Lambertian, it gives rise to a net torque

$$\mathbf{L}_{\text{thermal}} = -\frac{2}{3} \sum_{i=1}^{N} \mathscr{F}^i_{\text{thermal}} S_i (\mathbf{r}^i \times \mathbf{n}^i_B) \tag{3.170}$$

Thermal radiation torque can usually be neglected because the thermal flux is emitted roughly equally in all directions, so that the net torque is small.

Finally, Eqs. (3.168) and (3.170) ignore potential self-shadowing of concave spacecraft. If the configuration of the spacecraft is known a priori, self-shadowing can be taken into account by replacing S_i with the area of the flat plate that is visible to the Sun after accounting for shadowing. Modeling the effects of reflected radiation or thermal radiation from one surface striking another surface is an additional complication. Another drawback to Eq. (3.167) is that it is only valid for a collection of flat surfaces with uniquely defined outward normals. Most real spacecraft have some curved surfaces, and accurately approximating these surfaces by a collection of flat plates causes the size of the model to grow, increasing the computational burden.

3.3.6.5 Mass-Expulsion Torques

Translational momentum is the product $m\mathbf{v}$ of mass and velocity. We generally think of a force producing a rate of change of momentum $m\dot{\mathbf{v}}$. Mass-expulsion forces, on the other hand, are the result of a change of momentum $\mathbf{F}_{\text{mexp}} = -\dot{m}\mathbf{v}_{\text{rel}}$, where $\dot{m}$ is the rate at which mass is expelled, and $\mathbf{v}_{\text{rel}}$ is the velocity of the expelled mass relative to the spacecraft. Newton's third law of motion gives the negative sign, because this is a reaction force on the spacecraft. Another way to state this is to say that the mass-expulsion force reflects the conservation of momentum of the system consisting of the spacecraft and the expelled mass. Mass-expulsion forces provided by thrusters can be used to adjust the trajectories of spacecraft that require such corrections.

A mass-expulsion force will generally be accompanied by a torque

$$\mathbf{L}_{\text{mexp}} = \mathbf{r} \times \mathbf{F}_{\text{mexp}} = -\dot{m}\, \mathbf{r} \times \mathbf{v}_{\text{rel}} \tag{3.171}$$

where $\mathbf{r}$ is the vector from the spacecraft center of mass to the point where the mass is expelled. Undesirable mass-expulsion torques during orbit maneuvers can be minimized either by requiring the line of action of the thrust to pass through the spacecraft's center of mass or by using multiple thrusters whose torques cancel. It is impossible in practice to ensure exact cancelation, however.

Thrusters can also be used specifically as sources of torque. Attitude control thrusters are generally much smaller than orbit adjustment thrusters, because attitude control requires less force. An advantage of using thrusters for attitude control

is that they can be used anywhere, unlike magnetic torquers or gravity-gradient booms that require an ambient magnetic or gravitational field. They have the disadvantage of requiring expendable propellant, which can often be the element limiting the lifetime of a mission. Another disadvantage is that attitude control thrusters are accompanied by orbit-perturbing forces unless their forces are arranged in exact couples, equal and opposite pairs, which are impossible to attain in practice.

Use of thrusters for attitude control will be considered in more detail in Sect. 4.11 and Chap. 7, so this section will concentrate on mass-expulsion torques as a disturbance source. One source already mentioned is residual torques from orbit maneuvers, which can result from thruster misalignments or from impingement of thruster plumes on the spacecraft structure. Other common sources are outgassing of water vapor from the spacecraft structure during early stages of a mission or venting of cryogens. These can be minimized by arranging the vents to provide cancelation of the torques. Disturbances can also result from leaks of fuel, fuel pressurizing agents, or air from pressurized compartments, as on the International Space Station [18].

The Wilkinson Microwave Anisotropy Probe (WMAP) provided an interesting example of a mass-expulsion torque [25]. WMAP had a warm Sun-facing side and a cold side separated by a Sun shield of radius 2.5 m (see Fig. 7.4). Shortly after launch, WMAP executed three highly elliptical orbits with periods of approximately 7 days and with perigees on the sunlit side of the Earth. WMAP's attitude was inertially fixed prior to planned orbit adjustments at the perigees. About 40 min before the first perigee passage, the spacecraft angular momentum began to increase, peaking at about 2 Nms approximately 20 min before perigee and then decreasing. Various mechanisms for this anomalous torque were considered and rejected. The final explanation was that water vapor outgassing from the spacecraft had condensed on the cold side of the Sun shield as ice while WMAP was on the dark side of the Earth and had sublimated, first from one half of the Sun shield and then from the other, when the cold side was subjected to reflected sunlight from the Earth near perigee. The average velocity of the sublimated water molecules was estimated, assuming a temperature of 150 K, to be

$$v_{\text{rel}} = \sqrt{2k_B T / m_{H_2O}} = 370 \ \text{m/s} \tag{3.172}$$

where $k_B = 1.38 \times 10^{-23}$ J/K is the Boltzmann constant and $m_{H_2O} = 3 \times 10^{-26}$ kg is the mass of a water molecule. Assuming an average lever arm of $R = 1.1$ m, the quantity of sublimated ice required to explain the anomalous torque is only $\Delta m = \Delta H / R\, v_{\text{rel}} = 5$ g.

3.3.7 *Angular Momentum for Health Monitoring*

We have emphasized that internal momentum-exchange torques can lead to rapid variation of a spacecraft's angular velocity, but not of the system angular momentum. This insight led to an application of angular momentum conservation

for spacecraft failure detection [21]. A computer onboard the Hubble Space Telescope (HST) calculates the total system angular momentum $\mathbf{H}_B$ by means of Eqs. (3.139)–(3.141), with the angular velocity being sensed by the gyros and the wheel angular momentum computed using wheel tachometer data. The high torque of the reaction wheels can cause both the wheel angular momentum and the body angular momentum to change rapidly, but their vector sum only changes slowly. Subtracting easily computable gyroscopic, magnetic, and gravity-gradient torques from the rate of change of the computed system momentum gives an apparent disturbance torque:

$$\mathbf{L}_{\text{disturbance}} = \dot{\mathbf{H}}_B + \boldsymbol{\omega} \times \mathbf{H}_B - \mathbf{m} \times \mathbf{B} - \mathbf{L}_{gg} \tag{3.173}$$

with all the vectors computed in the spacecraft body frame. A large value of this disturbance torque indicates a failure of either a reaction wheel tachometer or a gyro. A tachometer failure could be identified by an independent test, so this angular momentum test was implemented onboard HST to identify gyro failures. The test initiated entry to a gyroless safehold mode three times in late 2002 and early 2003 [22].

3.3.8 Dynamics of Earth-Pointing Spacecraft

A great many spacecraft are pointed at the Earth to study its weather, climate, and resources. Thus it is useful to consider the special case of Earth-pointing spacecraft, whose body axes are closely aligned with the LVLH frame defined in Sect. 2.6.4. The attitude A_{BO} specifying the orientation of the spacecraft body axes to the axes of the LVLH frame, denoted by index O, is conveniently described by a $3-2-1$ Euler sequence of yaw $= \phi$, pitch $= \theta$, and roll $= \psi$ angles.

The dynamic equations give the motion relative to an inertial frame, so we write $A_{BI} = A_{BO} A_{OI}$ and use the Eq. (3.12) with the appropriate assignment of frame indices to find $\boldsymbol{\omega}_B^{BI}$. The matrix A_{BO} is given by Eq. (2.164), so Eq. (3.43) gives the components of $\boldsymbol{\omega}_B^{BO}$. The matrix A_{IO} is given by Eq. (2.79), so Eq. (3.3) can be used to find the angular velocity of the O frame with respect to the I frame:

$$\begin{aligned} -[\boldsymbol{\omega}_O^{OI}\times] = \dot{A}_{OI} A_{OI}^T = \dot{A}_{IO}^T A_{IO} &= \begin{bmatrix} \dot{\mathbf{o}}_{1I}^T \\ \dot{\mathbf{o}}_{2I}^T \\ \dot{\mathbf{o}}_{3I}^T \end{bmatrix} \begin{bmatrix} \mathbf{o}_{1I} & \mathbf{o}_{2I} & \mathbf{o}_{3I} \end{bmatrix} \\ &= \begin{bmatrix} \dot{\mathbf{o}}_{1I}\cdot\mathbf{o}_{1I} & \dot{\mathbf{o}}_{1I}\cdot\mathbf{o}_{2I} & \dot{\mathbf{o}}_{1I}\cdot\mathbf{o}_{3I} \\ \dot{\mathbf{o}}_{2I}\cdot\mathbf{o}_{1I} & \dot{\mathbf{o}}_{2I}\cdot\mathbf{o}_{2I} & \dot{\mathbf{o}}_{2I}\cdot\mathbf{o}_{3I} \\ \dot{\mathbf{o}}_{3I}\cdot\mathbf{o}_{1I} & \dot{\mathbf{o}}_{3I}\cdot\mathbf{o}_{2I} & \dot{\mathbf{o}}_{3I}\cdot\mathbf{o}_{3I} \end{bmatrix} \end{aligned} \tag{3.174}$$

Considering the derivatives of $\mathbf{o}_{iI}\cdot\mathbf{o}_{jI} = \delta_{ij}$ confirms that this 3×3 matrix is skew-symmetric. The inner products are frame-independent, but the subscript I is needed

to specify the frame used for differentiation. We substitute Eq. (2.78) and carry out some tedious but straightforward vector algebra to find the angular velocity of the LVLH frame relative to the inertial frame as

$$\boldsymbol{\omega}_O^{OI} = \begin{bmatrix} -\dot{\mathbf{o}}_{3I} \cdot \mathbf{o}_{2I} \\ \dot{\mathbf{o}}_{3I} \cdot \mathbf{o}_{1I} \\ -\dot{\mathbf{o}}_{2I} \cdot \mathbf{o}_{1I} \end{bmatrix} = \begin{bmatrix} (\dot{g}_3 \mathbf{r}_I + g_3 \mathbf{v}_I) \cdot \mathbf{o}_{2I} \\ -(\dot{g}_3 \mathbf{r}_I + g_3 \mathbf{v}_I) \cdot \mathbf{o}_{1I} \\ (\dot{g}_2 \mathbf{r}_I \times \mathbf{v}_I + g_2 \mathbf{r}_I \times \dot{\mathbf{v}}_I) \cdot \mathbf{o}_{1I} \end{bmatrix}$$

$$= \begin{bmatrix} 0 \\ -\|\mathbf{r}_I \times \mathbf{v}_I\| / \|\mathbf{r}_I\|^2 \\ \|\mathbf{r}_I\| (\mathbf{o}_{2I} \cdot \dot{\mathbf{v}}_I) / \|\mathbf{r}_I \times \mathbf{v}_I\| \end{bmatrix} \tag{3.175}$$

The roll component of this angular velocity is zero, and the yaw component is also zero if the spacecraft's acceleration $\dot{\mathbf{v}}_I$ is perpendicular to $\mathbf{o}_{2I}$, as it is for a purely central force. As shown in Sect. 10.4.3, a non-central force causes the orbit plane to precess, producing a small but finite yaw rotation rate. The pitch component of $\boldsymbol{\omega}_O^{OI}$ is by far the largest.

We can obtain the attitude motion in the general case by solving the dynamic equations from Sect. 3.3.2 with $\boldsymbol{\omega}_B^{BI}$ given by the procedure described above. However, it is useful to study the special case of uncontrolled attitude motion in a nearly circular Keplerian orbit with only small excursions from perfect alignment with the LVLH coordinate frame. Applying Eqs. (10.32), (10.39), (10.40), (10.15), and (10.43) of Chap. 10 to the pitch component of $\boldsymbol{\omega}_O^{OI}$ shows that

$$\|\mathbf{r}_I \times \mathbf{v}_I\| / \|\mathbf{r}_I\|^2 = n(1 - e^2)^{-3/2}(1 + e\cos\nu)^2 \tag{3.176}$$

where n is the mean motion, e is the eccentricity, ν is the true anomaly. Now we ignore all terms of higher than first order in the Euler angles, their rates, and the eccentricity, and we approximate the cosines of the Euler angles by unity and their sines by the angles themselves. With these approximations, Eqs. (3.12), (3.43), (2.164), and (3.176) give

$$\boldsymbol{\omega}_B^{BI} = \boldsymbol{\omega}_B^{BO} - \|\mathbf{r}_I \times \mathbf{v}_I\| / \|\mathbf{r}_I\|^2 \begin{bmatrix} \cos\theta \sin\phi \\ \cos\psi \cos\phi + \sin\psi \sin\theta \sin\phi \\ -\sin\psi \cos\phi + \cos\psi \sin\theta \sin\phi \end{bmatrix}$$

$$\approx \begin{bmatrix} \dot{\psi} \\ \dot{\theta} \\ \dot{\phi} \end{bmatrix} - n(1 + 2e\cos\nu) \begin{bmatrix} \phi \\ 1 \\ -\psi \end{bmatrix} \approx \begin{bmatrix} \dot{\psi} - n\phi \\ \dot{\theta} - n(1 + 2e\cos\nu) \\ \dot{\phi} + n\psi \end{bmatrix} \tag{3.177}$$

The first and third components of this equation exhibit the phenomenon of roll/yaw coupling. If we assume that the roll and yaw components of $\boldsymbol{\omega}_B^{BI}$ are exactly zero, we have $\dot{\psi} = n\phi$ and $\dot{\phi} = -n\psi$, with the solution

$$\psi(t) = \psi(t_0)\cos n(t - t_0) + \phi(t_0)\sin n(t - t_0) \tag{3.178a}$$

$$\phi(t) = \phi(t_0)\cos n(t - t_0) - \psi(t_0)\sin n(t - t_0) \tag{3.178b}$$

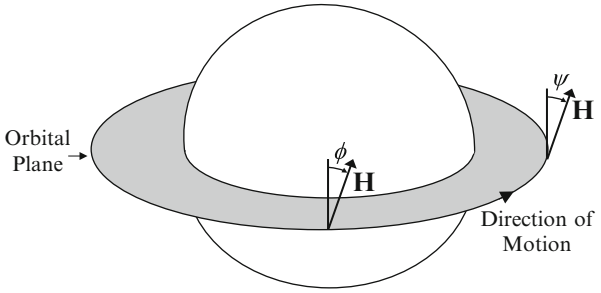

Fig. 3.6 Roll/yaw coupling

Thus a positive yaw becomes a positive roll one quarter orbit later and a negative yaw a quarter orbit after that, etc., which is why roll/yaw coupling is also known as quarter-orbit coupling. Figure 3.6 illustrates this effect, where **H** indicates the orientation of the spacecraft's total rotational angular momentum, which is assumed to be directed along the spacecraft's negative pitch axis but not exactly perpendicular to the orbit plane. Angular momentum conservation keeps the direction of this momentum fixed in inertial space, thereby ensuring that the roll and yaw components of $\boldsymbol{\omega}_B^{BI}$ remain small.

Let us now investigate the dynamic equations of motion, assuming that a reaction wheel, or possibly a combination of several wheels, provides a constant angular momentum bias h along the pitch axis. This is a common method for enhancing the roll/yaw coupling effect. Differentiating Eq. (3.177) and substituting Eq. (3.147) with $\mathbf{L}_B^w = 0$ as required by Eq. (3.146) gives

$$\begin{bmatrix} \ddot{\psi} - n\dot{\phi} \\ \ddot{\theta} + 2en^2 \sin\nu \\ \ddot{\phi} + n\dot{\psi} \end{bmatrix} = J_B^{-1}[\mathbf{L}_B - \boldsymbol{\omega}_B^{BI} \times (J_B \boldsymbol{\omega}_B^{BI} + h\mathbf{e}_2)] \tag{3.179}$$

This makes the further approximation $\dot{\nu} = n$, ignoring terms that would be of order e^2 in Eq. (3.179). Next assume that the body axes are principal axes and that the only significant external torque is the gravity-gradient torque, given by Eq. (3.157). Applying Eqs. (10.20) and (10.43) of Chap. 10 shows that

$$\frac{\mu}{r^3} = n^2 \left(\frac{1 + e\cos\nu}{1 - e^2} \right)^3 \tag{3.180}$$

We make the small-angle approximation for the trigonometric functions and ignore products of the eccentricity and the small angles, giving

$$\mathbf{L}_B = \mathbf{L}_{gg} = 3n^2 \begin{bmatrix} (J_3 - J_2)\psi \\ (J_3 - J_1)\theta \\ 0 \end{bmatrix} \tag{3.181}$$

Substituting Eq. (3.177) for the components of $\boldsymbol{\omega}_B^{BI}$ on the right side of Eq. (3.179), ignoring second-order terms in small quantities, and collecting terms gives

$$J_1\ddot{\psi} = n[4n(J_3 - J_2) + h]\psi + [n(J_1 - J_2 + J_3) + h]\dot{\phi} \tag{3.182a}$$

$$J_2\ddot{\theta} = 3n^2(J_3 - J_1)\theta - 2en^2 J_2 \sin\nu \tag{3.182b}$$

$$J_3\ddot{\phi} = n[n(J_1 - J_2) + h]\phi - [n(J_1 - J_2 + J_3) + h]\dot{\psi} \tag{3.182c}$$

The first property of these equations to notice is that pitch motion is decoupled from the roll and yaw motion. The pitch equation gives unstable motion with linear growth if $J_1 = J_3$ and unstable motion with exponential growth if $J_1 < J_3$, so pitch stability demands that $J_1 > J_3$. With the approximation $\dot{\nu} = n$, the solution for $J_1 > J_3$ is found to be

$$\theta = \theta_{\text{lib}} \cos(\omega_{\text{lib}} t + \alpha) + \frac{2en^2}{n^2 - \omega_{\text{lib}}^2} \sin\nu \tag{3.183}$$

where θ_{lib} and α are constants of integration, and

$$\omega_{\text{lib}} = n\sqrt{3(J_1 - J_3)/J_2} \tag{3.184}$$

is the libration frequency. The first term on the right side of Eq. (3.183) is the libration term, describing a pendular motion at the libration frequency. The second term gives a sinusoidal error at the orbit rate in a non-circular orbit, a result of the conflicting tendencies of rotational inertia to keep the pitch rate constant and of gravity-gradient torque to keep the yaw axis pointing along the nadir. This term grows very large near the pitch resonance case of $\omega_{\text{lib}} = n$, which must be avoided.[19] Its amplitude for the GEOS-3 spacecraft, with $e = 0.0054$, was 0.03° [27].

Now consider the roll/yaw dynamics expressed in Eqs. (3.182a) and (3.182c). The general solution of these two coupled second-order linear differential equation is a superposition of four components of the form

$$\begin{bmatrix} \psi(t) \\ \phi(t) \end{bmatrix} = \begin{bmatrix} \psi(0) \\ \phi(0) \end{bmatrix} e^{st} \tag{3.185}$$

with coefficients satisfying initial conditions. Substituting Eq. (3.185) into the roll/yaw dynamics gives a result expressible in matrix form as

$$\begin{bmatrix} J_1 s^2 + n[4n(J_2 - J_3) - h] & [n(J_2 - J_1 - J_3) - h]s \\ -[n(J_2 - J_1 - J_3) - h]s & J_3 s^2 + n[n(J_2 - J_1) - h] \end{bmatrix} \begin{bmatrix} \psi(0) \\ \phi(0) \end{bmatrix} e^{st} = 0 \tag{3.186}$$

[19] In the exact resonance case, Eq. (3.182b) has the growing solution $\theta = ent\cos\nu$.

This has a nontrivial solution only if the determinant of the 2×2 matrix is zero, which means that

$$J_1 J_3 s^4 + bs^2 + c = 0 \tag{3.187}$$

where

$$b = [n(J_2 - J_1 - J_3) - h]^2 + nJ_3[4n(J_2 - J_3) - h] + nJ_1[n(J_2 - J_1) - h] \tag{3.188a}$$

$$c = n^2[4n(J_2 - J_3) - h][n(J_2 - J_1) - h] \tag{3.188b}$$

Stable motion in roll and yaw requires that none of the roots of Eq. (3.187) has a positive real part. It is clear that if s is a root, then $-s$ is also a root, so stability requires all the roots to be purely imaginary numbers. The well-known solution of Eq. (3.187) is

$$2J_1 J_3 s^2 = -b \pm \sqrt{b^2 - 4J_1 J_3 c} \tag{3.189}$$

Both of the solutions, s^2, of Eq. (3.189) must be real and negative, with purely imaginary square roots, for roll/yaw stability. This will hold if and only if

$$c > 0 \quad \text{and} \quad b \geq 2\sqrt{J_1 J_3 c} \tag{3.190}$$

The first of these conditions is easier to satisfy; we see from Eq. (3.188b) that it requires

$$h > n \max\left(4(J_2 - J_3), (J_2 - J_1)\right) \quad \text{or} \tag{3.191a}$$

$$h < n \min\left(4(J_2 - J_3), (J_2 - J_1)\right) \tag{3.191b}$$

The second condition is harder to analyze, but a large enough positive or negative momentum bias h can provide roll/yaw stabilization for any moments of inertia, because b tends asymptotically to h^2, while c is asymptotic to $n^2 h^2$. In this asymptotic limit Eq. (3.189) becomes

$$2J_1 J_3 s^2 = -h^2\left(1 \pm \sqrt{1 - 4J_1 J_3 n^2/h^2}\right) \approx -h^2[1 \pm (1 - 2J_1 J_3 n^2/h^2)]$$

$$\approx \begin{cases} -2h^2 \\ -2J_1 J_3 n^2 \end{cases} \tag{3.192}$$

Comparison of the first root, $\omega = \sqrt{-s^2} = h/\sqrt{J_1 J_3}$, with Eq. (3.109) identifies this as a nutation frequency. The second root gives $\omega = n$, the frequency of the quarter-orbit roll/yaw coupling. These two frequencies do not separate as cleanly for general moments of inertia and bias angular momentum.

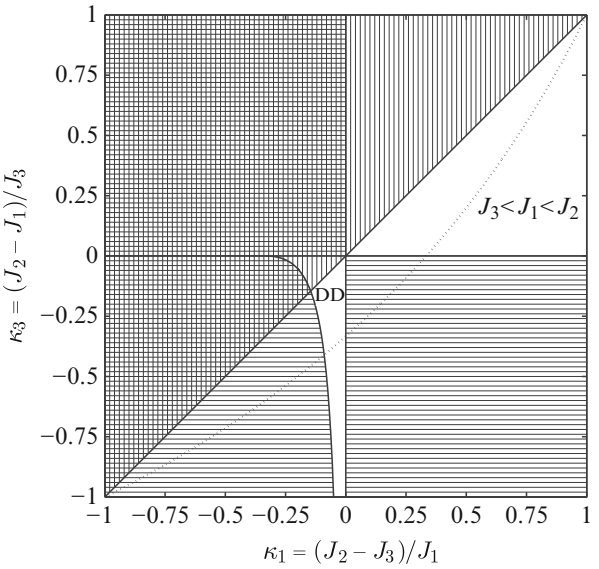

Fig. 3.7 Stability region map for gravity-gradient stabilization. *Unshaded areas* are regions of stable motion. The label DD identifies the DeBra-Delp region. *Areas with horizontal hatching* are unstable in roll and yaw; those with *vertical hatching* are unstable in pitch. The *dotted line* is the locus of the pitch orbital eccentricity resonance

We now investigate stability in the case of $h = 0$, a spacecraft with only gravity-gradient stabilization, which has been analyzed in detail. In this case, Eq. (3.188) reduces to

$$b = J_1 J_3 n^2 (1 + 3\kappa_1 + \kappa_1 \kappa_3) \tag{3.193a}$$

$$c = 4 J_1 J_3 n^4 \kappa_1 \kappa_3 \tag{3.193b}$$

where

$$\kappa_1 \equiv (J_2 - J_3)/J_1 \quad \text{and} \quad \kappa_3 \equiv (J_2 - J_1)/J_3 \tag{3.194}$$

The triangle inequality for principal moments of inertia, Eq. (3.73), implies that $-1 < \kappa_1 < 1$ and $-1 < \kappa_3 < 1$. Note that $\kappa_1 = 0$ for axially-symmetric inertia about the roll axis, $\kappa_3 = 0$ for symmetry about the yaw axis, and $\kappa_1 = \kappa_3$ for symmetry about the pitch axis.

Figure 3.7 shows the stability regions in terms of these variables in the $h = 0$ case. The requirements for roll/yaw stability in this case are simply

$$\kappa_1 \kappa_3 > 0 \quad \text{and} \quad 1 + 3\kappa_1 + \kappa_1 \kappa_3 \geq 4\sqrt{\kappa_1 \kappa_3} \tag{3.195}$$

These two requirements together demand that $\kappa_1 > -1/3$. Squaring the second requirement and collecting terms gives the quadratic inequality

$$(3+\kappa_3)^2\kappa_1^2 + 2(3-7\kappa_3)\kappa_1 + 1 \geq 0 \tag{3.196}$$

The roots of the equality are

$$\kappa_1 = (3+\kappa_3)^{-2}[(7\kappa_3 - 3 \pm 4\sqrt{3\kappa_3(\kappa_3-1)}] \tag{3.197}$$

Neither root is real if $0 < \kappa_3 < 1$, so the inequality of Eq. (3.196) is satisfied for any κ_1. Thus both parts of Eq. (3.195) are satisfied and roll/yaw stability is assured for

$$0 < \kappa_3 < 1 \quad \text{and} \quad 0 < \kappa_1 < 1 \tag{3.198}$$

The roots of Eq. (3.197) are real if $\kappa_3 < 0$, with the consequence that roll/yaw stability requires κ_1 to be either greater than the larger root or less than the smaller root. The smaller root is never greater than $-1/3$, though, so the only roll/yaw stability region for negative κ_3 is

$$-1 < \kappa_3 < 0 \quad \text{and} \quad (3+\kappa_3)^{-2}[(7\kappa_3 - 3 + 4\sqrt{3\kappa_3(\kappa_3-1)}] \leq \kappa_1 < 0 \tag{3.199}$$

This region, called the DeBra-Delp region [2], has $J_2 < J_3 < J_1$. It has rarely been employed in practice; almost all gravity-gradient-stabilized spacecraft are in the range of inertia values specified by Eq. (3.198), i.e. $J_3 < J_1 < J_2$.

It is always possible, and sometimes necessary, to supplement passive stabilization with active control using thrusters, magnetic torquers or reaction wheels. Active control effort can be minimized by starting with a stable configuration, however. A single pitch wheel can be used to control pitch and even to stabilize the pitch dynamics if $J_1 \leq J_3$. Roll/yaw coupling means that only two wheels are needed for three-axis control. Quite often the two wheels are slightly misaligned from the pitch axis so they can provide the momentum bias and also torques on two axes by commanding them in the same or opposite directions. GOES I-M, for instance, had two 51 Nms wheels with their spin axes tilted 1.66° in the positive and negative yaw directions from the negative pitch axis [24]. A much smaller 2.1 Nms wheel with its spin axis along yaw protected against failure of one of the two larger wheels.

Problems

3.1. Consider the Hill frame shown in Fig. 2.8. The deputy position expressed in Hill frame coordinates, denoted by $\mathbf{r}_{d_{\text{hill}}}$, is given by

$$\mathbf{r}_{d_{\text{hill}}} = \mathbf{r}_{c_{\text{hill}}} + \boldsymbol{\rho}_{\text{hill}} = (r_c + x)\mathbf{o}_r + y\,\mathbf{o}_\theta + z\,\mathbf{o}_h$$